Automatic Mode-Shifting Control Strategy With Input Voltage Feed-Forward for Full-Bridge-Boost DC–DC Converter Suitable for Wide Input Voltage Range

Chuan Yao, Xinbo Ruan, *Senior Member, IEEE*, and Xuehua Wang, *Member, IEEE*

***Abstract*—Full-bridge (FB)-boost converter is suitable for applications with wide input voltage range and galvanic isolation requirement, and a two-mode phase-shift (PS)-two-edge modulation (TEM) control scheme based on two modulation signals and one carrier can be used to achieve automatic mode shifting and high efficiency. In order to reduce the influence of the input voltage disturbance on the output voltage, the small-signal model of FB-boost converter is built and the input voltage feed-forward (IVFF) functions under different operating modes are derived in this paper. In view of the small-signal and large-signal control laws of the derived IVFF functions, the two-mode PS-TEM control schemes with small-signal and large-signal IVFF compensations are proposed, respectively. Both of them can realize automatic selection of operating modes and the corresponding IVFF compensations, and thus high efficiency and improved input transient response can be guaranteed. Besides, the IVFF function in boost mode is simplified for easy implementation, and the comparisons among the two-mode PS-TEM control schemes with small-signal, large-signal, and without IVFF compensations are presented in this paper. Finally, a 250–500-V input, 360-V output, and 6-kW-rated power prototype demonstrates the effectiveness of the proposed control schemes.**

***Index Terms*—Buck–boost converter, full-bridge (FB) converter, input voltage feed-forward (IVFF), large-signal, two-mode control.**

Nomenclature

FB	Full bridge.
PS	Phase shift.
RHP	Right-half-plane.
ZVS	Zero-voltage switching.
TEM	Two-edge modulation.
CCM	Continuous current mode.
TSBB	Two-switch buck boost.
IVFF	Input voltage feed forward.

Manuscript received January 5, 2014; revised March 9, 2014; accepted April 1, 2014. Date of publication April 16, 2014; date of current version October 15, 2014. This work was supported by the National Natural Science Foundation of China under Award 50837003 and Award 51007027, Jiangsu Province 333 Program for Excellent Talents under Award BRA2012141, and Fundamental Research Funds for the Central Universities under Award YAH12012. Recommended for publication by Associate Editor M. Ordonez.

C. Yao was with the State Key Laboratory of Advanced Electromagnetic Engineering and Technology, Huazhong University of Science and Technology, Wuhan 430074, China. He is now with the Wuhan Second Ship Design and Research Institute, Wuhan 430064, China (e-mail: yaochuan0707@hust.edu.cn).

X. Ruan is with the State Key Laboratory of Advanced Electromagnetic Engineering and Technology, Huazhong University of Science and Technology, Wuhan 430074, China, and is also with the Aero-Power Sci-Tech Center, Nanjing University of Aeronautics and Astronautics, Nanjing 210016, China (e-mail: ruanxb@nuaa.edu.cn).

X. Wang is with the State Key Laboratory of Advanced Electromagnetic Engineering and Technology, Huazhong University of Science and Technology, Wuhan 430074, China (e-mail: wang.xh@hust.edu.cn).

Color versions of one or more of the figures in this paper are available online at http://ieeexplore.ieee.org.

Digital Object Identifier 10.1109/TPEL.2014.2317795

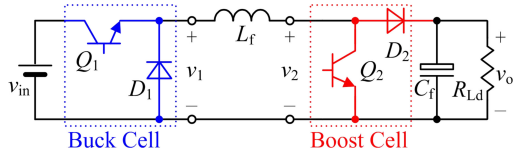

Fig. 1. TSBB converter.

I. Introduction

BUCK and boost converters are the two basic dc–dc converters. Buck converter has the ability of voltage step down, and its efficiency decreases with the increase of input voltage, whereas the boost converter has the ability of voltage step up and its efficiency increases with the increase of input voltage. Thus, neither of them is flexible in terms of input voltage range, nor can achieve high efficiency over a wide input voltage range [1]. Fig. 1 shows the two-switch buck–boost (TSBB) converter [2], where Q_1 and D_1 form the buck cell, and Q_2 and D_2 form the boost cell. The TSBB converter is a simplified cascade connection of the buck and boost converters, and it has the ability of voltage step up and step down. Compared with the basic converters, e.g., inverting buck–boost, Cuk, Zeta and SEPIC converters, the TSBB converter presents lower voltage stress of the power devices, fewer passive components, and positive output voltage [3]–[5], and has been widely used in the applications with wide input voltage range [6]–[9].

However, the TSBB converter has no ability on galvanic isolation. So, by replacing the buck cell with a full-bridge (FB) cell, a *FB-boost converter* is proposed in [10], as shown in Fig. 2, where switches $Q_1 \sim Q_4$, transformer T_r with turns ratio $k = W_2/W_1$, resonant inductor L_r (including the leakage inductor of T_r), and diodes $D_1 \sim D_4$ form the FB cell, and Q_b and D_b form the boost cell. The FB-boost converter is suitable for the applications where the input voltage range is wide while galvanic isolation is required, such as fuel-cell power systems. Moreover, in order to achieve high efficiency,

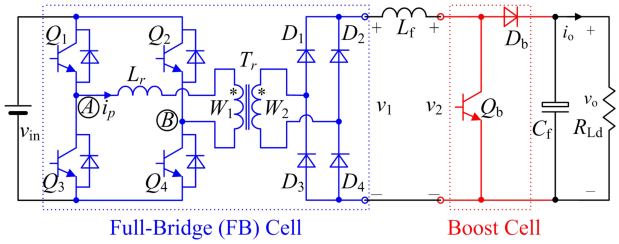

Fig. 2. FB-boost converter.

a two-mode phase-shift (PS)-two-edge modulation (TEM) control scheme is proposed for the FB-boost converter. When the input voltage reflecting to the secondary side of the transformer, i.e., $kv_{\rm in}$, is higher than the output voltage, $Q_{\rm b}$ of the boost cell is always off, and the FB cell is controlled to regulate the output voltage, and thus the FB-boost converter acts as a FB converter. This operating mode is defined as the *FB mode*. On the other hand, when $kv_{\rm in}$ is lower than the output voltage, the FB cell is operated with full duty cycle, and $Q_{\rm b}$ is controlled to regulate the output voltage, and thus the FB-boost converter acts as a boost converter. This operating mode is defined as the *boost mode*. In addition, PS control is adopted for the FB cell to realize zero-voltage switching, and FB and boost cells are leading-edge and trailing-edge modulated, respectively, to minimize the inductor current ripple, which is called the PS-TEM modulation. In order to achieve the two-mode operation over the whole load range, a third mode, i.e., *FB-boost mode*, is introduced. However, this *FB-boost mode* increases the conduction loss and switching loss of the converter, makes the mode-selection circuit complicated. So, this paper will propose an easily implemented automatic mode-shifting control scheme for the FB-boost converter based on two modulation signals with one carrier or one modulation signal with two carriers of the TSBB converter [11], [12]. With this proposed control scheme, automatic shifting between FB and boost modes and PS-TEM of the FB-boost converter are achieved, and the FB-boost mode is eliminated in theory, further improving the efficiency over the whole input voltage region.

When the FB-boost converter operates in continuous inductor current boost mode, a right-half-plane zero is presented. This will limit the bandwidth of the control loop and leads to a poor transient response, same as the TSBB converter [13], [14]. Especially, in the automatic mode-shifting control scheme, only one voltage regulator is used for both FB and boost modes, and it is often designed to have enough phase margin in boost mode by reducing the bandwidth of the control loop, thus the transient responses of this converter are deteriorated in the entire input voltage range, including FB and boost modes.

Input voltage feed-forward (IVFF) compensation [15]–[20] is an attractive approach for improving the transient response of a dc–dc converter, as it can eliminate the effect of the input voltage disturbance on the output voltage. In [21], an automatic mode-shifting control scheme with IVFF for the TSBB converter has been proposed to achieve high efficiency, automatic mode shifting, and improved transient response over the whole input voltage region. It should be noted that the IVFF function producing zero audio susceptibility for the TSBB converter derived in [21] is based on the small-signal model [22]–[25]. This small-signal control law can be easily implemented, but has the cost of accurate IVFF compensation and smooth mode shifting. Be different from [21], this paper analyzes a small-signal control law of the above-mentioned general IVFF method for the FB-boost converter with external resonant inductor, and a large-signal control law of the IVFF method, which can achieve more accurate IVFF compensation and smooth mode shifting will be derived. Moreover, automatic mode-shifting control schemes based on the small-signal and large-signal IVFF compensations are proposed for the FB-boost converter, respectively, achieving high efficiency, automatic and smooth mode shifting, and improved transient response over a wide input voltage range.

This paper is organized as follows. Section II introduces the automatic mode-shifting control scheme of the FB-boost converter, and Section III derives its small-signal models and IVFF functions under different operating modes. In Sections IV and V, the automatic mode-shifting control schemes with small-signal and large-signal IVFF compensations are proposed, respectively, achieving automatic selection of operating mode and the corresponding IVFF function simultaneously, and smooth mode shifting. The comparisons among the automatic mode-shifting control scheme with and without IVFF compensations are given in Section VI. Section VII presents the experimental results from a prototype with the proposed control schemes, and finally, Section VIII concludes this paper.

II. Two-Mode PS Two-Edge-Modulation Control Scheme With Automatic Mode-Shifting Ability

A. Two-Mode PS- TEM Control

When the FB-boost converter operates in continuous current mode (CCM), the output voltage is expressed as [10]

$$V_{\rm o} = \frac{D_{\rm y1\_eff}}{1-D_{\rm y2}}kV_{\rm in} = \frac{D_{\rm y1}-D_{\rm loss}}{1-D_{\rm y2}}kV_{\rm in} = \frac{D_{\rm y1}}{1-D_{\rm y2}}kV_{\rm in} - \frac{4k^2L_{\rm r}I_{\rm o}f_{\rm s}}{(1-D_{\rm y2})^2} \quad (1)$$

where $D_{\rm y1}$ and $D_{\rm y2}$ are the duty cycles of the FB and boost cells, respectively, $D_{\rm y1\_eff}$ is the effective duty cycle of the FB cell, $D_{\rm loss} = 4k^2L_{\rm r}I_{\rm o}f_{\rm s}/V_{\rm in}(1-D_{\rm y2})$ is the duty cycle loss resulted from the resonant inductor $L_{\rm r}$, $f_{\rm s}$ is the switching frequency of the FB cell, and $I_{\rm o}$ is the load current.

For the FB-boost converter with two-mode control, $D_{\rm y1}$ and $D_{\rm y2}$ are controlled independently, i.e., $D_{\rm y2}=0$, $D_{\rm y1}$ is controlled to regulate the output voltage in the FB mode, and $D_{\rm y1}=1$, $D_{\rm y2}$ is controlled to regulate the output voltage in the boost mode. Substituting $D_{\rm y1}=1$ and $D_{\rm y2}=0$ into (1), the input voltage at the shifting point of the two modes can be obtained as $kV_{\rm in\_b} = V_{\rm o} + 4k^2L_{\rm r}I_{\rm o}f_{\rm s} = V_{\rm o} + R_{\rm d}I_{\rm o}$, where $R_{\rm d} = 4k^2L_{\rm r}f_{\rm s}$ denotes the influence of $L_{\rm r}$ [26]. Thus, the output voltages of the FB-boost converter with two-mode control

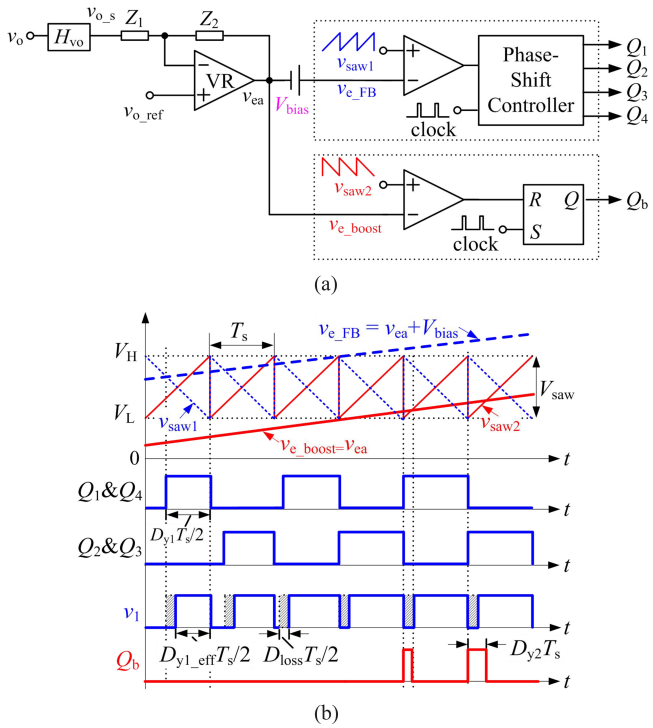

Fig. 3. Two-mode PS-TEM control scheme with automatic mode-switching ability. (a) Schematic diagram. (b) Key waveforms.

can be written as

$$V_o = \begin{cases} \dfrac{kV_{in}}{1-D_{y2}} - \dfrac{R_d I_o}{(1-D_{y2})^2}, D_{y1}=1\,(kV_{in} \le V_o + R_d I_o) \\ D_{y1} kV_{in} - R_d I_o, D_{y2}=0\,(kV_{in} > V_o + R_d I_o)\,. \end{cases} \tag{2}$$

As explained in Section I, the PS-TEM strategy is adopted here, i.e., PS control for the FB cell, and FB and boost cells are leading-edge and trialing-edge modulated, respectively. Overall, the control method with two-mode control and PS-TEM strategy is called the two-mode PS-TEM control scheme.

B. Two-Mode PS-TEM Control Scheme With Automatic Mode-Shifting Ability

By combining the two-mode control, PS-TEM, and the method with two modulation signals and one carrier together, the two-mode PS-TEM control scheme having automatic mode-shifting ability can be obtained. Fig. 3 shows the schematic diagram and key waveforms of the FB-boost converter under this control scheme. Here, PS control is adopted for the FB cell, Q_1 and Q_3 are the leading switches, Q_2 and Q_4 are the lagging switches, and Q_1 and Q_4 and Q_2 and Q_3 denote the simultaneous conduction of the diagonal switches Q_1 and Q_4, and Q_2 and Q_3, respectively. Moreover, v_{e_FB} and v_{e_boost} are the modulation signals, and v_{saw1} (leading edge) and v_{saw2} (trailing edge) are the carriers of FB and boost cells, respectively. It should be noted that the two carriers have the same amplitude and frequency, and their maximum, minimum, and peak-to-peak values are V_H, V_L, and $V_{saw} = V_H - V_L$, respectively.

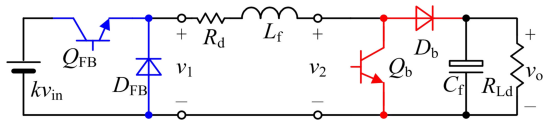

Fig. 4. Equivalent circuit of FB-boost converter.

In order to achieve the two-mode operation of the FB-boost converter, v_{e_FB} and v_{e_boost} in Fig. 3 are constructed as

$$\begin{cases} v_{e\_FB} = v_{ea} + V_{bias} \\ v_{e\_boost} = v_{ea} \end{cases} \tag{3}$$

where v_{ea} is the output signal of the voltage regulator, and V_{bias} is a dc bias voltage adding to v_{e_FB}. $V_{bias} = v_{e\_FB} - v_{e\_boost} \ge V_{saw}$ is the required condition to achieve the automatic shifting between FB and boost modes, and $V_{bias} = v_{e\_FB} - v_{e\_boost} = V_{saw}$ is the condition for smooth mode shifting, as explained in [21].

According to (3) with $V_{bias} = V_{saw}$, the principle of the control scheme shown in Fig. 3 can be described as follows: when $kV_{in} > V_o + R_d I_o$, v_{e_FB} will be within $[V_L, V_H]$, and it intersects v_{saw1} and determines D_{y1}; meanwhile, $v_{e\_boost} = v_{ea} = v_{e\_FB} - V_{saw} < V_L$, and thus $D_{y2} = 0$. Such case corresponds to the FB mode. When $kV_{in} < V_o + R_d I_o$, $v_{e\_boost} = v_{ea}$ will be within $[V_L, V_H]$, and it intersects v_{saw2} and determines D_{y2}; meanwhile, $v_{e\_FB} = v_{ea} + V_{saw} > V_H$, and thus $D_{y1} = 1$. Such case corresponds to the boost mode. When $kV_{in} = V_o + R_d I_o$, which is the shifting point of FB and boost modes, $v_{e\_boost} = V_L$, and thus $D_{y2} = 0$; meanwhile, $v_{e\_FB} = V_H$, and thus $D_{y1} = 1$.

III. IVFF of FB-Boost Converter With Two-Mode PS-TEM Control Scheme

A. Derivation of Small-Signal Model of FB-Boost Converter

Different from the TSBB converter, the FB-boost converter has a resonant inductor L_r, resulting in duty cycle loss and being equivalent to a resister $R_d = 4k^2 L_r f_s$ in series with the filter inductor L_f in the circuit [26]. Hence, an equivalent circuit of the FB-boost converter can be obtained from the TSBB converter by adding R_d in series with the inductor L_f and the input voltage equaling kv_{in}, as illustrated in Fig. 4, where Q_{FB} and D_{FB} are equivalent to the power switches and rectified diodes of FB cell, respectively. Referring to [27] and [28], the averaged switch model of FB-boost converter can be obtained by modeling the switch and diodes with a controlled current and voltage sources, whose values are equal to the average current flowing through the switch and the average voltages across the diode, respectively. Fig. 5(a) shows the specified averaged switch model of FB-boost converter, where $v_{in}, v_o, i_{Lf}, d_{y1}$, and d_{y2} are the input voltages, output voltages, inductor currents, and duty cycles of FB and boost cells, respectively. $i_{QFB} = d_{y1} i_{Lf}$ and $i_{Qb} = d_{y2} i_{Lf}$ are the average current flowing through switches Q_{FB} and Q_b, respectively, and $v_{DFB} = d_{y1} v_{in}$ and $v_{Db} = d_{y2} v_o$ are the average voltages across diodes D_{FB} and D_b, respectively.

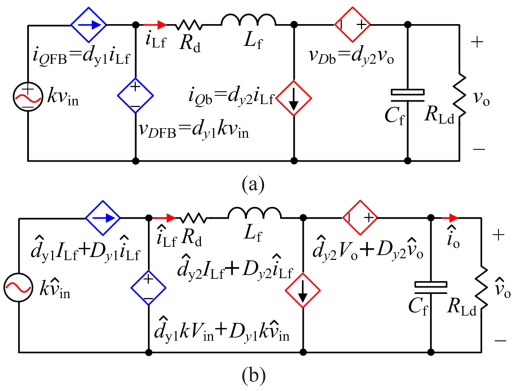

Fig. 5. Models of FB-boost converter. (a) Averaged switch model. (b) Small-signal model.

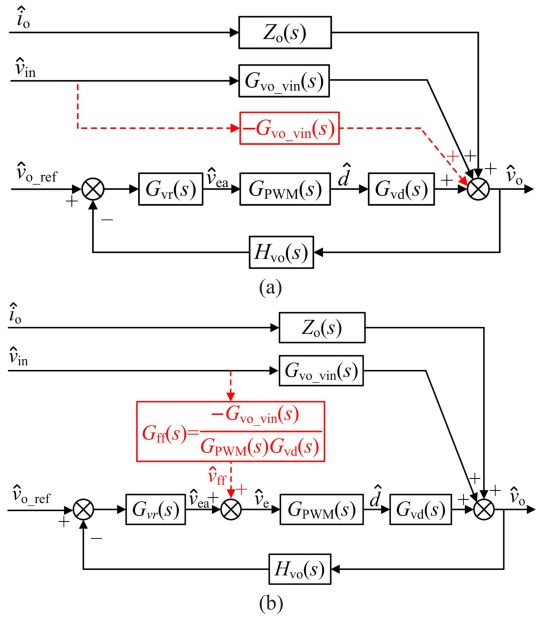

Fig. 6. Control block diagram with IVFF of a dc–dc converter. (a) Introduction of IVFF. (b) Equivalent transformation of IVFF.

Moreover, with small-signal assumption, the small-signal model of FB-boost converter can be obtained as illustrated in Fig. 5(b), by replacing the average values in Fig. 5(a) with their corresponding linearized ac terms [2]. In Fig. 5(b), the upper-case letter denotes the dc value, and the lower-case letter with cap (^) denotes the small-signal perturbation.

According to (2), setting $d_{y2}=0$, i.e., $D_{y2}=0$, $\hat{d}_{y2}=0$, and $d_{y1}=1$, i.e., $D_{y1}=1$, $\hat{d}_{y1}=0$ in Fig. 5(b), respectively, the small-signal models in FB and boost modes can be derived.

B. Derivation of IVFF Functions

Fig. 6(a) shows a general control block diagram of a dc–dc converter [2], where $G_{vd}(s)$, $G_{vo\_vin}(s)$, and $Z_o(s)$ are the transfer functions of duty ratio $\hat{d}$, input voltage $\hat{v}_{in}$, and load current $\hat{i}_o$ to the output voltage $\hat{v}_o$, respectively, $G_{vr}(s)$ is the transfer function of the voltage regulator, $G_{PWM}(s)$ is the transfer function of the pulse-width modulation (PWM) modulator, $\hat{v}_{o\_ref}$ is the output voltage reference, and $H_{vo}(s)$ is the sense gain of the output voltage. As seen, the disturbance of input voltage $\hat{v}_{in}$ affects the output voltage through the path with transfer function $G_{vo\_vin}(s)$. This effect can be eliminated by introducing an additional path with transfer function $-G_{vo\_vin}(s)$ from the input voltage to the output voltage, as illustrated with the dashed line shown in Fig. 6(a). Moving the output of $-G_{vo\_vin}(s)$ to the output of voltage regulator and the corresponding transfer function being changed to $G_{ff}(s)$, the control block is equivalently transformed to that shown in Fig. 6(b). The path from $\hat{v}_{in}$ to $\hat{v}_{ff}$ is called the IVFF path, and the IVFF function $G_{ff}(s)$ is

$$G_{ff}(s)=\frac{\hat{v}_{ff}}{\hat{v}_{in}}=-\frac{G_{vo\_vin}(s)}{G_{PWM}(s)G_{vd}(s)}. \tag{4}$$

As shown in Fig. 6(b), the output of $G_{ff}(s)$, i.e., $\hat{v}_{ff}$, is added to the output signal of the voltage regulator, i.e., $\hat{v}_{ea}$, forming the modulation signal $\hat{v}_e$.

By setting $D_{y2}=0$ and $\hat{d}_{y2}=0$ in Fig. 5(b), the small-signal model in FB mode can be obtained, and the transfer functions of duty ratio and input voltage to the output voltage, i.e., $G_{vd\_FB}(s)$ and $G_{vo\_vin\_FB}(s)$, can be, respectively, derived as

$$\begin{aligned}G_{vd\_FB}(s)&=\left.\frac{\hat{v}_o(s)}{\hat{d}_{y1}(s)}\right|_{\hat{v}_{in}=0}\\&=\frac{kV_{in}}{s^2L_fC_f+s\frac{L_f}{R_{Ld}}+sR_dC_f+\frac{R_d}{R_{Ld}}+1}\end{aligned} \tag{5}$$

$$\begin{aligned}G_{vo\_vin\_FB}(s)&=\left.\frac{\hat{v}_o(s)}{\hat{v}_{in}(s)}\right|_{\hat{d}_{y1}=0}\\&=\frac{1}{s^2L_fC_f+s\frac{L_f}{R_{Ld}}+sR_dC_f+\frac{R_d}{R_{Ld}}+1}\frac{V_o}{V_{in}}\left(1+\frac{R_d}{R_{Ld}}\right)\end{aligned} \tag{6}$$

where R_{Ld} is the resistor load of the FB-boost converter.

Likewise, by setting $D_{y1}=1$ and $\hat{d}_{y1}=0$ in Fig. 5(b), the small-signal model in boost mode can be obtained, and the transfer functions of duty ratio and input voltage to the output voltage, i.e., $G_{vd\_boost}(s)$ and $G_{vo\_vin\_boost}(s)$, can be, respectively, derived as

$$\begin{aligned}G_{vd\_boost}(s)&=\left.\frac{\hat{v}_o(s)}{\hat{d}_{y2}(s)}\right|_{\hat{v}_{in}=0}\\&=\frac{(1-D_{y2})V_o-\frac{(R_d+sL_f)V_o}{(1-D_{y2})R_{Ld}}}{s^2L_fC_f+s\frac{L_f}{R_{Ld}}+sR_dC_f+\frac{R_d}{R_{Ld}}+(1-D_{y2})^2}\end{aligned} \tag{7}$$

$$\begin{aligned}G_{vo\_vin\_boost}(s)&=\left.\frac{\hat{v}_o(s)}{\hat{v}_{in}(s)}\right|_{\hat{d}_{y1}=0}\\&=\frac{k(1-D_{y2})}{s^2L_fC_f+s\frac{L_f}{R_{Ld}}+sR_dC_f+\frac{R_d}{R_{Ld}}+(1-D_{y2})^2}.\end{aligned} \tag{8}$$

TABLE I
SPECIFICATIONS OF THE PROTOTYPE

Specifications	Symbol	Value
Input voltage	V_{in}	250-500 V
Output voltage	V_o	360 V
Output power	P_o	6 kW
Full load current/ resistor	I_{o_N}/ R_{Ld}	16.7 A/ 21.6 Ω

TABLE II
PARAMETERS OF THE PROTOTYPE

Parameter	Symbol	Value
Filter capactior	C_f	4080 μF
Filter inductor	L_f	320 μH
Turns ratio of T_r	k	11: 11
Reasonant inductor	L_r	5 μH
Switching frequency	f_s, f_{s_b}	50 kHz, 100 kHz
Switches	Q_1~Q_4, Q_b	SPW47N60C3
Rectfied diodes	D_1~D_4	DSEI60-06
Boost diode	D_b	SDP30S120
Sense gain of the input voltage	H_{vin}	1/100
Sense gain of the output voltage	H_{vo}	1/144
Peak-to-peak value of the carrier	V_{saw}	2.5 V

As described in Section II-B, the carriers for the FB and boost cells have same amplitude and frequency, so the PWM modulator transfer functions in FB and boost modes are the same, and its specific expression is

$$G_{\mathrm{PWM}}(s)=\frac{\hat{d}(s)}{\hat{v}_e(s)}=\frac{1}{V_{saw}}. \tag{9}$$

By substituting (5), (6) and (9) into (4), the IVFF function in FB mode, i.e., $G_{ff\_FB}(s)$ can be expressed as

$$\begin{aligned} G_{ff\_FB}(s) &= -\frac{V_o}{kV_{in}^2}\left(1+\frac{R_d}{R_{Ld}}\right)V_{saw} \\ &= -\frac{V_o+R_dI_o}{kV_{in}^2}V_{saw}. \end{aligned} \tag{10}$$

Similarly, by substituting (7)–(9) into (4), the IVFF function in boost mode, i.e., $G_{ff\_boost}(s)$ can be expressed as

$$\begin{aligned} G_{ff\_boost}(s) &= -\frac{kV_{saw}}{V_o\left[1-\dfrac{4V_oI_o(R_d+sL_f)}{\left(kV_{in}+\sqrt{k^2V_{in}^2-4R_dV_oI_o}\right)^2}\right]} \\ &= -\frac{k}{V_o\left[D_{en1}-D_{en2}(s)\right]}V_{saw} \end{aligned} \tag{11}$$

where $D_{en1}=1-4V_oR_dI_o/(kV_{in}+\sqrt{k^2V_{in}^2-4R_dV_oI_o})^2$ and $D_{en2}(s)=4V_oI_oL_fs/(kV_{in}+\sqrt{k^2V_{in}^2-4R_dV_oI_o})^2$.

As seen in (11), $D_{en2}(s)$ is the function of frequency, whose coefficient, i.e., $4V_oI_oL_f/(kV_{in}+\sqrt{k^2V_{in}^2-4R_dV_oI_o})^2$, reaches its maximum value at full load and minimum input voltage. According to the specifications and parameters of the prototype listed in Tables I and II given in Section VII, the magnitudes of D_{en1} and $D_{en2}(s)$ with full load current $I_{o\_N}=16.7$ A and minimum input voltage $V_{in\_min}=250$ V are depicted in Fig. 7. It is known that the input voltage of the fuel-cell power system has a wide variation range, but fluctuates at low frequency, and thus $|D_{en2}(s)| << |D_{en1}|$, as shown in Fig. 7. Hence, (11) can be simplified as

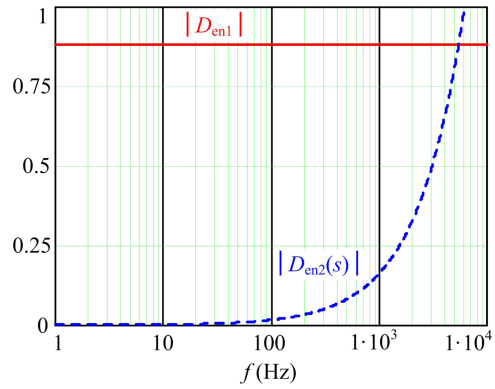

Fig. 7. Magnitudes of D_{en1} and $D_{en2}(s)$ as the functions of frequency.

$$G_{ff\_boost}(s)=-\frac{k}{2V_o}\left(1+\frac{kV_{in}}{\sqrt{k^2V_{in}^2-4R_dV_oI_o}}\right)V_{saw}. \tag{12}$$

As seen from (10) and (12), it is known that the IVFF functions for the FB and boost modes are different. So, it is important to ensure that the FB-boost converter can operate in correct mode with correct IVFF function and shift between the two modes automatically. Moreover, as explained in [24] and [25], the derived IVFF function has two control laws, i.e., small-signal and large-signal control laws. Thus, the following sections of this paper will discuss the automatic mode-shifting control schemes with IVFF based on the two control laws, respectively.

IV. TWO-MODE PS-TEM CONTROL SCHEME WITH SMALL-SIGNAL IVFF COMPENSATION

According to (10) and (12), the IVFF functions in FB and boost modes depend on the input voltage V_{in} and load current I_o at quiescent operation point, and corresponding to different values in different operating modes. To make a distinction, the input voltage and load current at quiescent operation point are defined as V_{in_FB} and I_{o_FB} in $G_{ff\_FB}(s)$, and V_{in_B} and I_{o_B} in $G_{ff\_boost}(s)$, respectively. Therefore, the IVFF functions of FB and boost modes can be rewritten as

$$\begin{cases} G_{ff\_FB}(s)=-\dfrac{V_o+R_dI_{o\_FB}}{kV_{in\_FB}^2}V_{saw} \\ G_{ff\_boost}(s)=-\dfrac{k}{2V_o}\left(1+\dfrac{kV_{in\_B}}{\sqrt{k^2V_{in\_B}^2-4R_dV_oI_{o\_B}}}\right)V_{saw}. \end{cases} \tag{13}$$

Considering the critical output current at the boundary of CCM is designed to be 10% of full load. Thus, according to Table I, the load range of FB-boost converter operated in CCM can be obtained as $[10\%I_{o\_N},\ 100\%I_{o\_N}]=[1.67,\ 16.7$ A], whose middle value is set as the load current at quiescent operation

point for the IVFF functions, i.e., $I_{o\_FB} = I_{o\_B} = 55\%I_{o\_N} \approx 9$ A. Based on this, the input voltage at the shifting point of FB and boost modes with the load current equaling $55\%I_{o\_N}$ can be written as $kV_{in\_b} = V_o + 55\%R_dI_{o\_N}$, corresponding to $V_{in\_b} = 369$ V. Meanwhile, the input voltage ranges of FB and boost mode can be obtained as [369, 500 V] and [250, 369 V], whose middle values are set as the input voltages of quiescent operation point in $G_{ff\_FB}(s)$ and $G_{ff\_boost}(s)$, respectively, i.e., $V_{in\_FB} = (369 + 500)/2 \approx 435$ V and $V_{in\_B} = (250 + 369)/2 \approx 310$ V.

According to (4) and (13), the output signals of the IVFF functions under different modes can be obtained as

$$\begin{cases} v_{ff\_FB} = G_{ff\_FB}v_{in} - \dfrac{V_o + R_dI_{o\_FB}}{kV_{in\_FB}^2}V_{saw}v_{in} \\ v_{ff\_boost} = G_{ff\_boost}v_{in} \\ -\dfrac{k}{2V_o}\left(1 + \dfrac{kV_{in\_B}}{\sqrt{k^2V_{in\_B}^2 - 4R_dV_oI_{o\_B}}}\right)V_{saw}v_{in}. \end{cases} \tag{14}$$

As seen in Fig. 6(b), the modulation signal v_e is the sum of the output signals of the IVFF function and the voltage regulator, i.e., $v_e = v_{ff} + v_{ea}$. Therefore, according to (3) and (14), the modulation signals of the FB-boost converter under the two-mode PS-TEM control scheme with IVFF compensation can be expressed as

$$\begin{cases} v_{e\_FB} = v_{ff\_FB} + v_{ea} + V_{bias} \\ = -\dfrac{V_o + R_dI_{o\_FB}}{kV_{in\_FB}^2}V_{saw}v_{in} + v_{ea} + V_{bias} \\ v_{e\_boost} = v_{ff\_boost} + v_{ea} \\ = -\dfrac{k}{2V_o}\left(1 + \dfrac{kV_{in\_B}}{\sqrt{k^2V_{in\_B}^2 - 4R_dV_oI_{o\_B}}}\right) \\ \times V_{saw}v_{in} + v_{ea}. \end{cases} \tag{15}$$

As discussed in Section II-B, $v_{e\_FB} - v_{e\_boost} \geq V_{saw}$ should be satisfied for the two-mode operation and automatic mode shifting. Thus, V_{bias} in (15) can be derived as

$$\begin{aligned} &V_{bias} \\ &\geq V_{saw} - kV_{saw}v_{in} \\ &\quad \times \left(\frac{1}{2V_o} + \frac{kV_{in\_B}}{2V_o\sqrt{k^2V_{in\_B}^2 - 4R_dV_oI_{o\_B}}} - \frac{V_o + R_dI_{o\_FB}}{k^2V_{in\_FB}^2}\right) \\ &= V_{saw} - kV_{saw}v_{in}(A_1 - A_2) \end{aligned} \tag{16}$$

where $A_1 = 1/2V_o + kV_{in\_B}\Big/2V_o\sqrt{k^2V_{in\_B}^2 - 4R_dV_oI_{o\_B}}$ and $A_2 = (V_o + R_dI_{o\_FB})/k^2V_{in\_FB}^2$.

It is known that $kV_{in\_B} > \sqrt{k^2V_{in\_B}^2 - 4R_dV_oI_{o\_B}}$, which means that A_1 in (16) satisfies $A_1 > 1/V_o > 1/(V_o + R_dI_{o\_FB})$, leading to

$$\begin{aligned} A_1 - A_2 &> \frac{1}{V_o + R_dI_{o\_FB}} - \frac{V_o + R_dI_{o\_FB}}{k^2V_{in\_FB}^2} \\ &= (V_o + R_dI_{o\_FB})\left[\frac{1}{(V_o + R_dI_{o\_FB})^2} - \frac{1}{k^2V_{in\_FB}^2}\right]. \end{aligned} \tag{17}$$

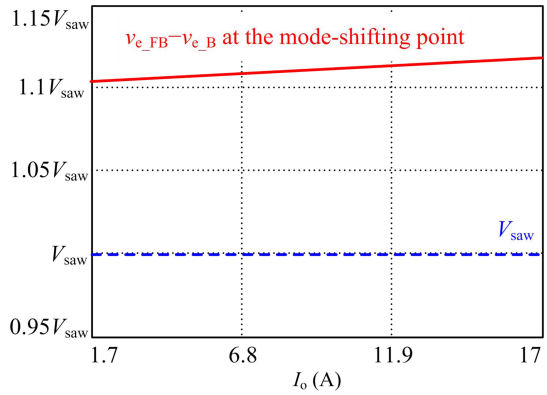

Fig. 8. $v_{e\_FB} - v_{e\_boost}$ at the mode-shifting point as the function of I_o.

As aforementioned, $V_o + R_dI_{o\_FB}$ is the input voltage at the shifting point of FB and boost modes with the load current at quiescent operation point of FB-boost converter, i.e., the minimum value in the input voltage region of FB mode with this load current, and yet kV_{in_FB} is the middle value of this input voltage region. Consequently, $kV_{in\_FB} > V_o + R_dI_{o\_FB}$ and $A_1 - A_2 > 0$ are satisfied, which means that the right-hand side of (16) decreases with the input voltage v_{in}, and it gets its maximum value at the minimum input voltage V_{in_min}. So, here, V_{bias} is set to this maximum value for automatic selection and nearly smooth shifting between FB and boost modes with the corresponding IVFF functions, i.e.,

$$V_{bias} = V_{saw} - kV_{saw}V_{in\_min}(A_1 - A_2). \tag{18}$$

By substituting (18) into (15), the final modulation signals of the FB-boost converter can be expressed as

$$\begin{cases} v_{e\_FB} = v_{ff\_FB} + v_{ea} + V_{bias} \\ = -\dfrac{V_o + R_dI_{o\_FB}}{kV_{in\_FB}^2}V_{saw}v_{in} + v_{ea} + V_{saw} \\ \quad -kV_{saw}V_{in\_min}(A_1 - A_2) \\ v_{e\_boost} = v_{ff\_boost} + v_{ea} \\ = -\dfrac{k}{2V_o}\left(1 + \dfrac{kV_{in\_B}}{\sqrt{k^2V_{in\_B}^2 - 4R_dV_oI_{o\_B}}}\right)V_{saw}v_{in} + v_{ea}. \end{cases} \tag{19}$$

Furthermore, substitution of the input voltage $kv_{in} = V_o + R_dI_o$ into (19) can obtain the value of $v_{e\_FB} - v_{e\_boost}$ at the mode-shifting point, which is the function of I_o, as depicted in Fig. 8. As seen, $v_{e\_FB} - v_{e\_boost}$ at the mode-shifting point is not equal to V_{saw}, but has maximum value equaling 1.13 V_{saw}, which can be treated as nearly smooth shifting between FB and boost modes.

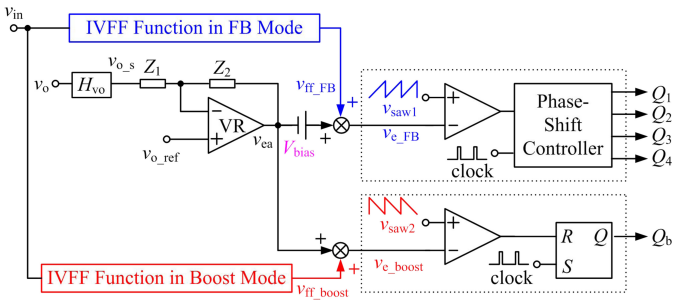

Fig. 9. Schematic of FB-boost converter under the two-mode PS-TEM control with IVFF.

As analyzed before, the modulation signals in (19) can achieve automatic selection and shifting of the operating mode and the corresponding IVFF function, simultaneously. It should be explained that the quiescent operation point of the FB-boost converter with wide input voltage range is changed timely. However, the input voltage and load currents of the quiescent operation point in the IVFF functions, i.e., $V_{\mathrm{in\_FB}}$, $I_{\mathrm{o\_FB}}$, $V_{\mathrm{in\_B}}$, and $I_{\mathrm{o\_B}}$ in (19) are all fixed, so it is also called that the IVFF functions are based on the small-signal control law, and the method with the modulation signals in (19) is defined as the two-mode PS-TEM control scheme with small-signal IVFF compensation, and the corresponding schematic diagram is shown in Fig. 9.

V. Two-Mode PS-TEM Control Scheme With Large-Signal IVFF Compensation

This section will discuss the implementation of the IVFF function derived with a large-signal control law and a two-mode PS-TEM control scheme with large-signal IVFF compensation.

According to Fig. 6, the small-signal duty ratio of the dc–dc converter with IVFF compensation can be expressed as

$$\hat{d} = \hat{v}_e G_{\mathrm{PWM}}(s) = \frac{\hat{v}_{\mathrm{ff}} + \hat{v}_{\mathrm{ea}}}{V_{\mathrm{saw}}} = \frac{G_{\mathrm{ff}}(s)\,\hat{v}_{\mathrm{in}}}{V_{\mathrm{saw}}} + \frac{\hat{v}_{\mathrm{ea}}}{V_{\mathrm{saw}}}. \quad (20)$$

As seen, the duty ratio with IVFF compensation is provided by the output signals of the IVFF function and the voltage regulator, i.e., $\hat{v}_{\mathrm{ff}}$ and $\hat{v}_{\mathrm{ea}}$, together. Once the input voltage disturbance $\hat{v}_{\mathrm{in}}$ happens, the duty ratio from $\hat{v}_{\mathrm{ff}}$ will be changed in a fast way to prevent the change of the output voltage, and the duty ratio from $\hat{v}_{\mathrm{ea}}$ is zero.

By substituting (10) and (12) into (20), the small-signal duty ratios with IVFF compensation in FB mode and boost mode can be written as

$$\begin{cases} \hat{d}_{\mathrm{y1}} = -\dfrac{V_{\mathrm{o}} + R_{\mathrm{d}} I_{\mathrm{o}}}{kV_{\mathrm{in}}^2}\hat{v}_{\mathrm{in}} + \dfrac{\hat{v}_{\mathrm{ea}}}{V_{\mathrm{saw}}} \\ \hat{d}_{\mathrm{y2}} = -\dfrac{k}{2V_{\mathrm{o}}}\left(1 + \dfrac{kV_{\mathrm{in}}}{\sqrt{k^2V_{\mathrm{in}}^2 - 4R_{\mathrm{d}}V_{\mathrm{o}}I_{\mathrm{o}}}}\right)\hat{v}_{\mathrm{in}} + \dfrac{\hat{v}_{\mathrm{ea}}}{V_{\mathrm{saw}}}. \end{cases} \quad (21)$$

It is known that (20) is also suitable for the steady state of the dc–dc converter, i.e., the duty ratio at the steady state are composed of the output signals of the IVFF compensation and voltage regulator, corresponding expression is

$$D = \frac{V_{\mathrm{ff}}}{V_{\mathrm{saw}}} + \frac{V_{\mathrm{ea}}}{V_{\mathrm{saw}}} \quad (22)$$

where V_{ff} and V_{ea} are the output signals from the IVFF compensation and the voltage regulator at the steady state, respectively.

Referring to (2), the duty ratios for keeping the output voltage constant at the steady state of FB and boost modes can be obtained, and both of them are provided by their corresponding output signals of the IVFF compensation, i.e.,

$$\begin{cases} \dfrac{V_{\mathrm{ff\_FB}}}{V_{\mathrm{saw}}} = \dfrac{V_{\mathrm{o}} + R_{\mathrm{d}} I_{\mathrm{o}}}{kV_{\mathrm{in}}} \\ \dfrac{V_{\mathrm{ff\_boost}}}{V_{\mathrm{saw}}} = 1 - \dfrac{kV_{\mathrm{in}} + \sqrt{k^2V_{\mathrm{in}}^2 - 4R_{\mathrm{d}}V_{\mathrm{o}}I_{\mathrm{o}}}}{2V_o} \end{cases} \quad (23)$$

where $V_{\mathrm{ff\_FB}}$ and $V_{\mathrm{ff\_boost}}$ are the output signals of the IVFF compensation at the steady state of FB and boost modes, respectively.

Substituting (23) into (22), the duty ratios with IVFF compensation at the steady state for different operating modes can be written as

$$\begin{cases} D_{\mathrm{y1}} = \dfrac{V_{\mathrm{ff\_FB}}}{V_{\mathrm{saw}}} + \dfrac{V_{\mathrm{ea}}}{V_{\mathrm{saw}}} = \dfrac{V_{\mathrm{o}} + R_{\mathrm{d}} I_{\mathrm{o}}}{kV_{\mathrm{in}}} + \dfrac{V_{\mathrm{ea}}}{V_{\mathrm{saw}}} \\ D_{\mathrm{y2}} = \dfrac{V_{\mathrm{ff\_boost}}}{V_{\mathrm{saw}}} + \dfrac{V_{\mathrm{ea}}}{V_{\mathrm{saw}}} \\ \qquad = 1 - \dfrac{kV_{\mathrm{in}} + \sqrt{k^2V_{\mathrm{in}}^2 - 4R_{\mathrm{d}}V_{\mathrm{o}}I_{\mathrm{o}}}}{2V_o} + \dfrac{V_{\mathrm{ea}}}{V_{\mathrm{saw}}}. \end{cases} \quad (24)$$

As seen, when the input voltage at the quiescent operation point, i.e., V_{in}, is changed, the duty ratio from the output signals of the IVFF compensation will be changed timely to keep the output voltage constant. Likewise, the duty ratio from the voltage regulator is zero, i.e., $V_{\mathrm{ea}}/V_{\mathrm{saw}} = 0$, in theory.

Furthermore, by adding the duty ratio in same operating mode between (21) and (24), the large-signal forms of the duty ratios with IVFF compensation in FB and boost modes can be obtained as eq. (25) shown at the bottom of the next page.

It can be observed that B_1, B_2, and C in (25) all satisfy the Taylor expansion with dc and linear ac terms, i.e.,

$$f(Y + \hat{y}) = f(y)|_{y=Y} + \hat{y}\frac{\partial f(y)}{\partial y}|_{y=Y} \quad (26)$$

where $f(y)$ is the function requiring Taylor expansion, and Y and $\hat{y}$ are the dc and ac components of the independent variable y, respectively.

Referring to (26), the expressions in (25) can be rewritten as

$$\begin{cases} d_{\mathrm{y1}} = \dfrac{V_{\mathrm{o}} + R_{\mathrm{d}} I_{\mathrm{o}}}{k\left(V_{\mathrm{in}} + \hat{v}_{\mathrm{in}}\right)} + \dfrac{V_{\mathrm{ea}} + \hat{v}_{\mathrm{ea}}}{V_{\mathrm{saw}}} = \dfrac{V_{\mathrm{o}} + R_{\mathrm{d}} I_{\mathrm{o}}}{k v_{\mathrm{in}}} + \dfrac{v_{\mathrm{ea}}}{V_{\mathrm{saw}}} \\ d_{\mathrm{y2}} = 1 - \dfrac{k\left(V_{\mathrm{in}} + \hat{v}_{\mathrm{in}}\right) + \sqrt{k^2\left(V_{\mathrm{in}} + \hat{v}_{\mathrm{in}}\right)^2 - 4R_{\mathrm{d}} V_{\mathrm{o}} I_{\mathrm{o}}}}{2V_o} \\ \qquad + \dfrac{V_{\mathrm{ea}} + \hat{v}_{\mathrm{ea}}}{V_{\mathrm{saw}}} \\ \qquad = 1 - \dfrac{k v_{\mathrm{in}} + \sqrt{k^2 v_{\mathrm{in}}^2 - 4R_{\mathrm{d}} V_{\mathrm{o}} I_{\mathrm{o}}}}{2V_o} + \dfrac{v_{\mathrm{ea}}}{V_{\mathrm{saw}}} \end{cases} \tag{27}$$

where $v_{\mathrm{in}} = V_{\mathrm{in}} + \hat{v}_{\mathrm{in}}$ is the input voltage, $v_{\mathrm{ea}} = V_{\mathrm{ea}} + \hat{v}_{\mathrm{ea}}$ is the output signal of the voltage regulator, $(V_{\mathrm{o}} + R_{\mathrm{d}} I_{\mathrm{o}})/k v_{\mathrm{in}}$ and $1 - \left(k v_{\mathrm{in}} + \sqrt{k^2 v_{\mathrm{in}}^2 - 4R_{\mathrm{d}} V_{\mathrm{o}} I_{\mathrm{o}}}\right)\Big/ 2V_o$ are the duty ratios provided by the output signals of the IVFF compensation in FB and boost modes, respectively, all of which are their large-signal forms, composed of their dc and small-signal ac components. So, the IVFF compensation in (27) is called the large-signal IVFF compensation, or the IVFF function based on the large-signal control law.

As seen in (27), d_{y2} has a square-root term, i.e., $\sqrt{k^2 v_{\mathrm{in}}^2 - 4R_{\mathrm{d}} V_{\mathrm{o}} I_{\mathrm{o}}} = k v_{\mathrm{in}} \sqrt{1 - 4R_{\mathrm{d}} V_{\mathrm{o}} I_{\mathrm{o}} / k^2 v_{\mathrm{in}}^2}$, which requires rather complicated implementation. Let $x = 1/k^2 v_{\mathrm{in}}^2$ and $a = 4R_{\mathrm{d}} V_{\mathrm{o}} I_{\mathrm{o}}$, the square-root term aforementioned has $\sqrt{1 - 4R_{\mathrm{d}} V_{\mathrm{o}} I_{\mathrm{o}} / k^2 v_{\mathrm{in}}^2} = \sqrt{1 - ax}$, whose Taylor expansion without nonlinear ac terms at $x = 0$ is

$$\begin{aligned} \sqrt{1 - 4R_{\mathrm{d}} V_{\mathrm{o}} I_{\mathrm{o}} / k^2 v_{\mathrm{in}}^2} = \sqrt{1 - ax} &\approx 1 - \frac{a}{2} x \\ &= 1 - \frac{2R_{\mathrm{d}} V_{\mathrm{o}} I_{\mathrm{o}}}{k^2 v_{\mathrm{in}}^2}. \end{aligned} \tag{28}$$

Fig. 10 plots the curves of (28) as the function of input voltage with and without Taylor expansion in the full load condition. As seen, the curves are much close to each other, and thus the expansion in (28) is reasonable.

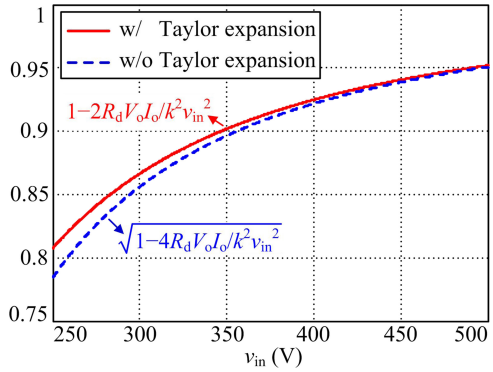

Fig. 10. Curves of $\sqrt{1 - 4R_{\mathrm{d}} V_{\mathrm{o}} I_{\mathrm{o}} / k^2 v_{\mathrm{in}}^2}$ with and without Taylor expansion.

According to (28), (27) can be simplified as

$$\begin{cases} d_{\mathrm{y1}} = \dfrac{V_{\mathrm{o}} + R_{\mathrm{d}} I_{\mathrm{o}}}{k v_{\mathrm{in}}} + \dfrac{v_{\mathrm{ea}}}{V_{\mathrm{saw}}} \\ d_{\mathrm{y2}} = 1 - \dfrac{k v_{\mathrm{in}}}{V_{\mathrm{o}}} + \dfrac{R_{\mathrm{d}} I_{\mathrm{o}}}{k v_{\mathrm{in}}} + \dfrac{v_{\mathrm{ea}}}{V_{\mathrm{saw}}}. \end{cases} \tag{29}$$

According to (29), the modulation signals with large-signal IVFF compensation in FB and boost modes can be derived as

$$\begin{cases} v_{\mathrm{e\_FB}} = d_{\mathrm{y1}} V_{\mathrm{saw}} = \left(\dfrac{V_{\mathrm{o}} + R_{\mathrm{d}} I_{\mathrm{o}}}{k v_{\mathrm{in}}}\right) V_{\mathrm{saw}} + v_{\mathrm{ea}} \\ \quad = v_{\mathrm{ff\_FB}} + v_{\mathrm{ea}} \\ v_{\mathrm{e\_boost}} = d_{\mathrm{y2}} V_{\mathrm{saw}} = \left(1 - \dfrac{k v_{\mathrm{in}}}{V_{\mathrm{o}}} + \dfrac{R_{\mathrm{d}} I_{\mathrm{o}}}{k v_{\mathrm{in}}}\right) V_{\mathrm{saw}} + v_{\mathrm{ea}} \\ \quad = v_{\mathrm{ff\_boost}} + v_{\mathrm{ea}}. \end{cases} \tag{30}$$

It can be known from (30) that $v_{\mathrm{ff\_FB}}$ and $v_{\mathrm{ff\_boost}}$ are dependent on the input voltage and load current. According to Tables I and II listed in Section VII, $v_{\mathrm{ff\_FB}}$ and $v_{\mathrm{ff\_boost}}$ as the function of input voltage at different load condition are shown in Fig. 11. As seen, $v_{\mathrm{ff\_FB}}$ and $v_{\mathrm{ff\_boost}}$ in (30) are insensitive to the load current. For a compromise solution, I_{o} in (30) is set as a fixed value, which equals $55\% I_{\mathrm{o\_N}}$ here.

$$\begin{cases} d_{\mathrm{y1}} = D_{\mathrm{y1}} + \hat{d}_{\mathrm{y1}} = \underbrace{\dfrac{V_{\mathrm{o}} + R_{\mathrm{d}} I_{\mathrm{o}}}{k V_{\mathrm{in}}} - \dfrac{V_{\mathrm{o}} + R_{\mathrm{d}} I_{\mathrm{o}}}{k V_{\mathrm{in}}^2} \hat{v}_{\mathrm{in}}}_{\mathrm{B_1}} + \underbrace{\dfrac{V_{\mathrm{ea}}}{V_{\mathrm{saw}}} + \dfrac{\hat{v}_{\mathrm{ea}}}{V_{\mathrm{saw}}}}_{C} \\ d_{\mathrm{y2}} = D_{\mathrm{y2}} + \hat{d}_{\mathrm{y2}} \\ \quad = \underbrace{1 - \dfrac{k V_{\mathrm{in}} + \sqrt{k^2 V_{\mathrm{in}}^2 - 4R_{\mathrm{d}} V_{\mathrm{o}} I_{\mathrm{o}}}}{2V_o} - \dfrac{k}{2V_{\mathrm{o}}} \left(1 + \dfrac{k V_{\mathrm{in}}}{\sqrt{k^2 V_{\mathrm{in}}^2 - 4R_{\mathrm{d}} V_{\mathrm{o}} I_{\mathrm{o}}}}\right) \hat{v}_{\mathrm{in}}}_{\mathrm{B_2}} \\ \quad + \underbrace{\dfrac{V_{\mathrm{ea}}}{V_{\mathrm{saw}}} + \dfrac{\hat{v}_{\mathrm{ea}}}{V_{\mathrm{saw}}}}_{C} \end{cases} \tag{25}$$

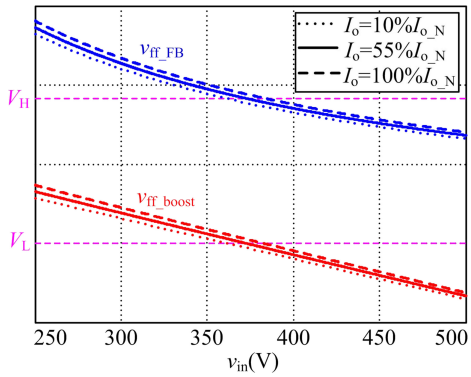

Fig. 11. $v_{\mathrm{ff\_FB}}$ and $v_{\mathrm{ff\_boost}}$ as the functions of v_{in} at different I_{o}.

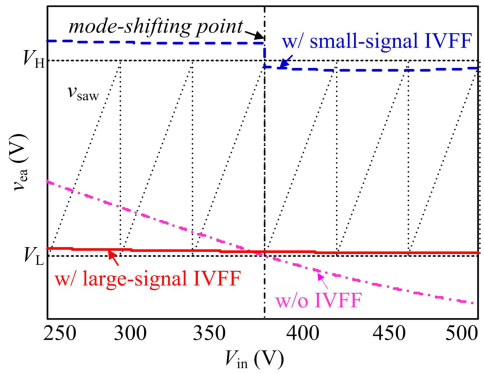

Fig. 12. Comparison of v_{ea} between the two-mode PS-TEM control with and without IVFF compensations.

It also can be observed that $v_{\mathrm{e\_FB}}$ and $v_{\mathrm{e\_boost}}$ in (30) satisfy

$$v_{\mathrm{e\_FB}} - v_{\mathrm{e\_boost}} = \left(\frac{V_{\mathrm{o}}}{kv_{\mathrm{in}}} + \frac{kv_{\mathrm{in}}}{V_o} - 1\right) V_{\mathrm{saw}} \geq V_{\mathrm{saw}}. \quad (31)$$

Thus, as described in Section II, $v_{\mathrm{e\_FB}}$ and $v_{\mathrm{e\_boost}}$ in (30) can achieve automatic selection and shifting of operating modes and the corresponding IVFF compensation, simultaneously. Moreover, substitution of the input voltage at the mode-shifting point, i.e., $kv_{\mathrm{in}} = V_{\mathrm{o}} + R_{\mathrm{d}} I_{\mathrm{o}}$ into (30), $v_{\mathrm{e\_FB}} - v_{\mathrm{e\_boost}}$ at the mode-shifting point can be gotten, and its maximum value is $1.002\, V_{\mathrm{saw}}$, which can be treated as smooth shifting between FB and boost modes. The control method with modulation signals in (30) is defined as the two-mode PS-TEM control scheme with large-signal IVFF compensation, whose schematic diagram can also be illustrated with Fig. 9 and $V_{\mathrm{bias}} = 0$.

By using Taylor expansion for $v_{\mathrm{ff\_FB}}$ and $v_{\mathrm{ff\_boost}}$ in (30), the corresponding linear ac terms are $\hat{v}_{\mathrm{ff\_FB}}$ and $\hat{v}_{\mathrm{ff\_boost}}$, respectively. Moreover, according to (4), the IVFF function for the large-signal IVFF compensation can be derived as

$$\begin{cases} G_{\mathrm{ff\_FB}}(s) = -\dfrac{V_{\mathrm{o}} + R_{\mathrm{d}} I_{\mathrm{o}}}{kV_{\mathrm{in}}^2} V_{\mathrm{saw}} \\ G_{\mathrm{ff\_boost}}(s) = \left(-\dfrac{k}{V_o} - \dfrac{R_{\mathrm{d}} I_{\mathrm{o}}}{kV_{\mathrm{in}}^2}\right) V_{\mathrm{saw}}. \end{cases} \quad (32)$$

As seen, the expressions of $G_{\mathrm{ff\_FB}}(s)$ in (13) and (32) are the same, and the difference is that the quiescent operation point of $G_{\mathrm{ff\_FB}}(s)$ in (32) is not fixed, but changed timely. Likewise, the expressions of $G_{\mathrm{ff\_boost}}(s)$ in (13) and (32) are the same in theory. However, due to the simplified expression, i.e., (28) is introduced, the $G_{\mathrm{ff\_boost}}(s)$ in (32) is different from it in (13), but still has timely changed quiescent operation points.

VI. Comparisons Between the Two-Mode PS-TEM Control Scheme With and Without IVFF Compensations

A. Output Signal of the Voltage Regulator

In steady state, the relationship between the modulation signal and the duty ratio under different operating modes shown in Fig. 3(b) can be expressed as

$$\begin{cases} \dfrac{v_{\mathrm{e\_FB}} - V_{\mathrm{L}}}{D_{\mathrm{y1}} T_{\mathrm{s}}} = \dfrac{V_{\mathrm{saw}}}{T_{\mathrm{s}}}, v_{\mathrm{e\_boost}} < V_{\mathrm{L}} \ (kV_{\mathrm{in}} > V_{\mathrm{o}} + R_{\mathrm{d}} I_{\mathrm{o}}) \\ \dfrac{v_{\mathrm{e\_boost}} - V_{\mathrm{L}}}{D_{\mathrm{y2}} T_{\mathrm{s}}} = \dfrac{V_{\mathrm{saw}}}{T_{\mathrm{s}}}, v_{\mathrm{e\_FB}} > V_{\mathrm{H}} \ (kV_{\mathrm{in}} \leq V_{\mathrm{o}} + R_{\mathrm{d}} I_{\mathrm{o}}). \end{cases} \quad (33)$$

Substituting the duty ratio expressions shown in (2) into (33) yields

$$\begin{cases} v_{\mathrm{e\_FB}} = \left(\dfrac{V_{\mathrm{o}} + R_{\mathrm{d}} I_{\mathrm{o}}}{kV_{\mathrm{in}}}\right) V_{\mathrm{saw}} + V_{\mathrm{L}}, v_{\mathrm{e\_boost}} < V_{\mathrm{L}} \\ (kV_{\mathrm{in}} > V_{\mathrm{o}} + R_{\mathrm{d}} I_{\mathrm{o}}) \\ v_{\mathrm{e\_boost}} = \left(1 - \dfrac{kV_{\mathrm{in}} + \sqrt{k^2 V_{\mathrm{in}}^2 - 4R_{\mathrm{d}} V_{\mathrm{o}} I_{\mathrm{o}}}}{2V_o}\right) V_{\mathrm{saw}} \\ \qquad + V_{\mathrm{L}}, v_{\mathrm{e\_FB}} > V_{\mathrm{H}} \\ (kV_{\mathrm{in}} \leq V_{\mathrm{o}} + R_{\mathrm{d}} I_{\mathrm{o}}). \end{cases} \quad (34)$$

As seen in (34), the modulation signals under the two-mode PS-TEM control scheme are the functions of input voltage and load current. After the input voltage and load current being known, the corresponding modulation signal will be determined, no matter the IVFF compensation being incorporated or not. Thus, combining (34) with (3), (19), and (30), respectively, the output signals of the voltage regulator under the two-mode PS-TEM control scheme without, with small-signal, and with large-signal IVFF compensations can be obtained, corresponding to the dot dashed, dashed, and solid lines shown in Fig. 12, respectively. It can be seen that the variation of v_{ea} with IVFF compensation over the whole input voltage range, especially for that with large-signal IVFF compensation, is much smaller than that without IVFF compensation, which implies that the IVFF mainly regulated the output voltage, extremely alleviating the task of the voltage regulator, improving the input transient response. It should be noted that the v_{ea} with small-signal IVFF compensation at the mode-shifting point shown in Fig. 12 has a small leap, leading to nearly smooth shifting between FB and boost modes, as described in Section IV. However, there is no leap for the v_{ea} with large-signal IVFF compensation at the mode-shifting point, and a smooth mode shifting is achieved.

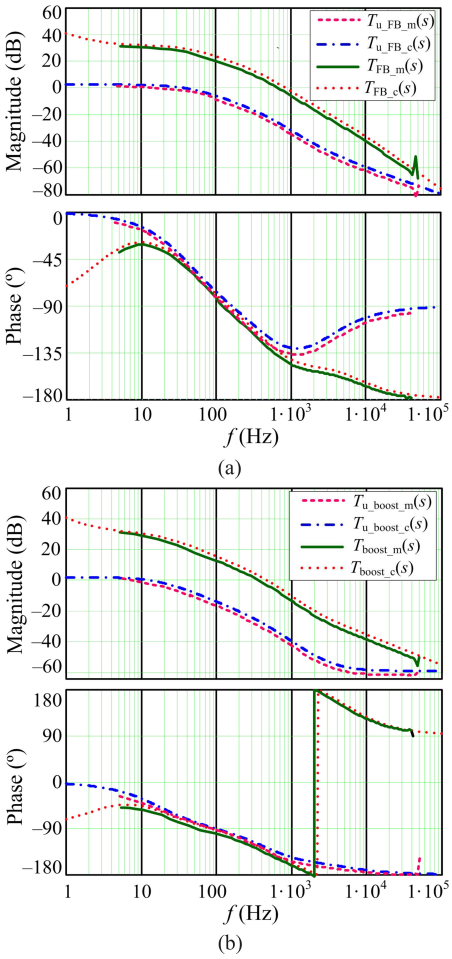

Fig. 13. Bode diagrams of the loop gains under different operating modes. (a) $V_{\mathrm{in\_max}} = 500$ V, FB mode. (b) $V_{\mathrm{in\_min}} = 250$ V, boost mode.

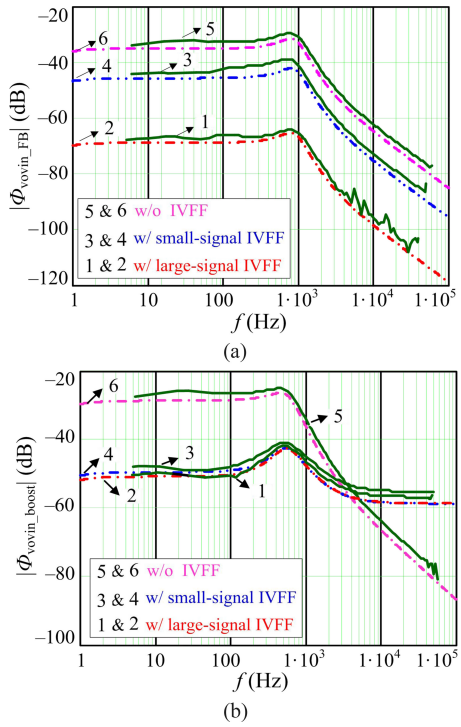

Fig. 14. Bode diagrams of the input to output voltage transfer function. (a) $V_{\mathrm{in\_max}} = 500$ V, FB mode. (b) $V_{\mathrm{in\_min}} = 250$ V, boost mode.

B. Input-to-Output Voltage Transfer Function

According to Fig. 6, the loop gain of a dc–dc converter is

$$T(s) = G_{\mathrm{vr}}(s) G_{\mathrm{PWM}}(s) G_{\mathrm{vd}}(s) H_{\mathrm{vo}}(s). \tag{35}$$

Referring to the design consideration in [21], the bode diagrams of the uncompensated and compensated loop gains for FB-boost converter under different operating modes can be obtained, as shown in Fig. 13, where (a) gives the bode diagram in FB mode with the maximum input voltage $V_{\mathrm{in\_max}} = 500$ V, and (b) gives the bode diagram in boost mode with the minimum input voltage $V_{\mathrm{in\_min}} = 250$ V. Specifically, the dot-dashed and dashed lines in Fig. 13(a) are the calculated and measured uncompensated loop-gains in FB mode, i.e., $T_{\mathrm{u\_FB\_c}}(s)$ and $T_{\mathrm{u\_FB\_m}}(s)$, and the dotted and solid lines are the calculated and measured compensated loop-gains in this mode, i.e., $T_{\mathrm{FB\_c}}(s)$ and $T_{\mathrm{FB\_m}}(s)$, respectively. Similarly, the dot-dashed and dashed lines in Fig. 13(b) are the calculated and measured uncompensated loop-gains in boost mode, i.e., $T_{\mathrm{u\_boost\_c}}(s)$ and $T_{\mathrm{u\_boost\_m}}(s)$, and the dotted and solid lines are the calculated and measured compensated loop gains in this mode, i.e., $T_{\mathrm{boost\_c}}(s)$ and $T_{\mathrm{boost\_m}}(s)$, respectively. As seen, the calculated and measured loop gains are close to each other.

It should be emphasized that the FB-boost converter under different operating modes share one regulator, i.e., $G_{\mathrm{vr}}(s)$, which is considered in boost mode in this paper, and its specific expression is

$$G_{\mathrm{vr}}(s) = \frac{30s + 500}{s\left(\frac{s}{5000} + 1\right)}. \tag{36}$$

It can be seen from Fig. 13 that enough phase margins are ensured in both FB and boost modes, but the bandwidths of the two modes are very low, leading to poor dynamic performance over the entire input voltage range. Hence, it is very necessary to use the IVFF compensation to improve the input voltage transient response of the FB-boost converter with the voltage regulator expressed in (36).

According to Fig. 6, the closed-loop input-to-output voltage transfer function with IVFF compensation, $\Phi_{\mathrm{vo\_vin}}(s)$, can be expressed as

$$\begin{aligned}\Phi_{\mathrm{vo\_vin}}(s) &= \frac{\hat{v}_{\mathrm{o}}(s)}{\hat{v}_{\mathrm{in}}(s)} \\ &= \frac{G_{\mathrm{vo\_vin}}(s) + G_{\mathrm{ff}}(s) G_{\mathrm{PWM}}(s) G_{\mathrm{vd}}(s)}{1 + T(s)}.\end{aligned} \tag{37}$$

Substituting $G_{\mathrm{ff}}(s)$ expressed in (13) and (32) into (37), the magnitudes of $\Phi_{\mathrm{vo\_vin}}(s)$ with small-signal and large-signal IVFF compensations can be obtained, as the lines 2 and 4 shown in Fig. 14, respectively, where lines 1 and 3 are corresponding to their measured magnitudes, and Fig. 14(a) and (b) are corresponding to the converter operated in FB and boost modes,

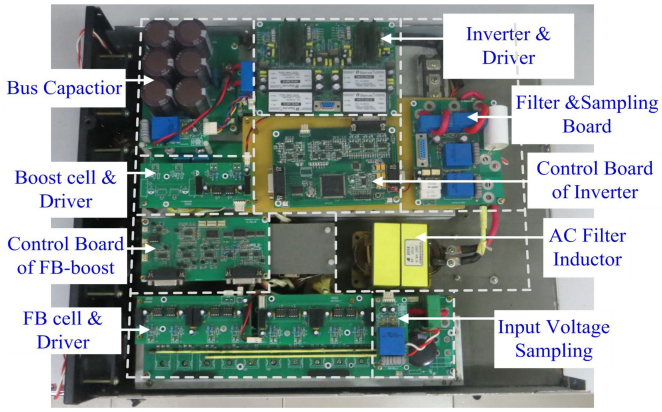

Fig. 15. Photograph of the prototype for the FB-boost converter.

respectively. In addition, the lines 6 and 5 shown in Fig. 14 are the calculated and measured $\Phi_{\mathrm{vo\_vin}}(s)$ without IVFF compensation, i.e., $G_{\mathrm{ff}}(s) = 0$ in (37), respectively. As seen, the calculated and measured magnitudes of $\Phi_{\mathrm{vo\_vin}}(s)$ are in accordance with each other on the whole. It also can be seen from Fig. 14 that the ability on suppressing the effect of the input voltage disturbance on the output voltage for the FB-boost converter with IVFF compensation is improved obviously, no matter in FB or boost mode. Moreover, compared with the small-signal IVFF compensation, the large-signal IVFF compensation, whose quiescent operation point is changed timely, has better effectiveness on IVFF over the entire input voltage region, especially in FB mode. Besides, it also can be seen that the effectiveness of IVFF in boost mode is remarkable in the low-frequency range. The reason is that the IVFF functions in boost mode, including its small-signal and large-signal control laws, are both based on (12), which is (11) neglecting the term changed with frequency. When the frequency is lower, (12) is more close to (11), leading to more accurate IVFF function and better effectiveness.

C. Implementation

Referring to (19) and (30), it is known that only proportion operation of input voltage is included in the small-signal IVFF compensation, yet in the large-signal IVFF compensation, the division operation of input voltage is involved, requiring relatively complicated realization.

VII. Experimental Verification

In order to verify the effectiveness of the proposed control schemes, a power prototype is fabricated, whose specifications and parameters are listed in Tables I and II, respectively. Please be noted that the filter capacitor C_{f} is designed when the FB-boost converter operated as the front-end dc–dc converter in a two-stage power system, and it needs to provide all of the pulsating power of the down-stream dc–ac inverter. Fig. 15 gives a photograph of the prototype for the FB-boost converter, where its main circuit, controlling circuit, sampling circuit, and driving circuit are included.

Figs. 16 and 17 show the diagrams of the FB-boost converter under the two-mode PS-TEM control scheme with small-signal and large-signal IVFF compensations, respectively, where one PS controller UC3895 and one PWM controller UC3525 are employed for controlling FB and boost cells, and v_{saw1} and v_{saw2} are their trailing-edge modulated carriers with same amplitude and frequency. In addition, Q_{1_g} to Q_{4_g} are the drive signals from UC3895, and $Q_{\mathrm{b\_g}}$ is the drive signal from UC3525. Specifically, Q_{1_g} and Q_{3_g} are the drive signals for Q_1 and Q_3, i.e., the leading switches of FB cell, Q_{2_g} and Q_{4_g} are the drive signals for Q_2 and Q_4, i.e., the lagging switches of the FB cell, and $Q_{\mathrm{b\_g}}$ is the drive signal for Q_{b}. In order to achieve the TEM strategy with FB cell being leading-edge modulated and boost cell being trailing-edge modulated, the drive signals Q_{1_g} and Q_{3_g} are sent to the NOR gate, i.e., NOR #1, giving a pulse signal with the pulsewidth equal to the dead time of Q_{1_g} and Q_{3_g}. This pulse signal is then sent to the *SYNC* pin of UC3525 as the synchronous signal for the boost cell, as described in [10].

In Fig. 16, the input voltage is sensed by the resistor $R_{\mathrm{s3}} = 50$ kΩ, $R_{\mathrm{s4}} = 200$ Ω, and the sensor LV25-P with primary to secondary current ratio $k_{\mathrm{c}} = 2.5$, and through a voltage follower composed by O/A #2. Then, the sensed input voltage, i.e., $v_{\mathrm{in\_s}} = v_{\mathrm{in}} k_{\mathrm{c}} R_{\mathrm{s4}}/R_{\mathrm{s3}} = v_{\mathrm{in}}/100$, is connected to inverting pins of UC3895 E/A #1 through R_6 and UC3525 E/A #2 through R_{10}, respectively. In addition, the sensed output voltage $v_{\mathrm{o\_s}}$, which is obtained from the divider resistors R_{s1}, R_{s2}, and voltage follower O/A #1, is connected to the inverting pin of E/A #3 through R_1, and the reference voltage $v_{\mathrm{o\_ref}}$, which is obtained from V_{REF2}-pin of UC3525 with divider resistors $R_{12} = R_{13} = 10$ kΩ, is connected to the noninverting pin of E/A #3. Consequently, E/A #3, $R_1 = 10$ kΩ, $R_2 = 300$ kΩ, $C_1 = 100$ pF, and $C_2 = 200$ nF compose the voltage regulator, whose output signal v_{ea} is connected to the noninverting pins of UC3895 E/A #1 through R_4 and UC3525 EA#2 through R_8. For the E/A #1, a dc bias voltage, which is obtained from the V_{REF1} pin with divider resistors R_3 and R_5, is also connected to its noninverting pin. In Fig. 16, the output signals of E/A #1 and E/A #2 are the modulation signals of FB and boost cells, and their specific expressions are

$$\begin{cases} v_{\mathrm{e\_FB}} = \left(\dfrac{R_7}{R_6}+1\right)\dfrac{R_5}{R_4R_5+R_3R_4+R_3R_5} \\ \qquad\qquad \times (R_4V_{\mathrm{REF1}}+R_3v_{\mathrm{ea}}) - \dfrac{R_7}{R_6}v_{\mathrm{in\_s}} \\ v_{\mathrm{e\_boost}} = \left(\dfrac{R_{11}}{R_{10}}+1\right)\dfrac{R_9}{R_8+R_9}v_{\mathrm{ea}} - \dfrac{R_{11}}{R_{10}}v_{\mathrm{in\_s}}. \end{cases} \tag{38}$$

Combining (19), (38), and $V_{\mathrm{saw}} = 2.5$ V, the values of $R_3 \sim R_{11}$ in Fig. 16 can be obtained as $R_3 = 2.4$ kΩ, $R_4 = 1$ kΩ, $R_5 = 11$ kΩ, $R_6 = 10$ kΩ, $R_7 = 5$ kΩ, $R_8 = R_{11} = 36$ kΩ, $R_9 = R_{10} = 50$ kΩ.

Referring to Figs. 16 and 17, they have similar configuration, and the difference is that the sensed input voltage $v_{\mathrm{in\_s}}$ and a dc bias voltage from V_{REF1} pin with divider resistors R_8 and R_9 are connected to a Multiplier&&Divider circuit, whose output signal $v_{\mathrm{in\_div}} = (R_8V_{\mathrm{REF1}})^2/[(R_8+R_9)^2 v_{\mathrm{in\_s}}]$ is connected to the noninverting pins of E/A #1 through R_3, and E/A #2 through R_{12}, achieving the required division operation of the large-signal IVFF

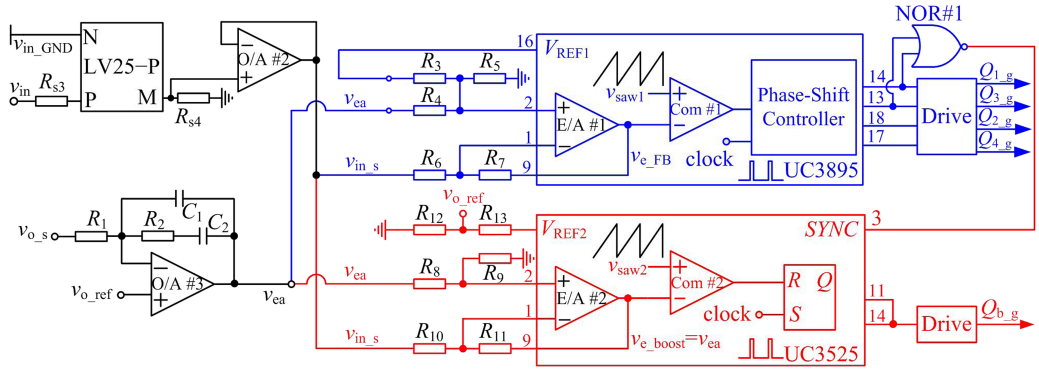

Fig. 16. Two-mode PS-TEM control with small-signal IVFF F for FB-boost converter.

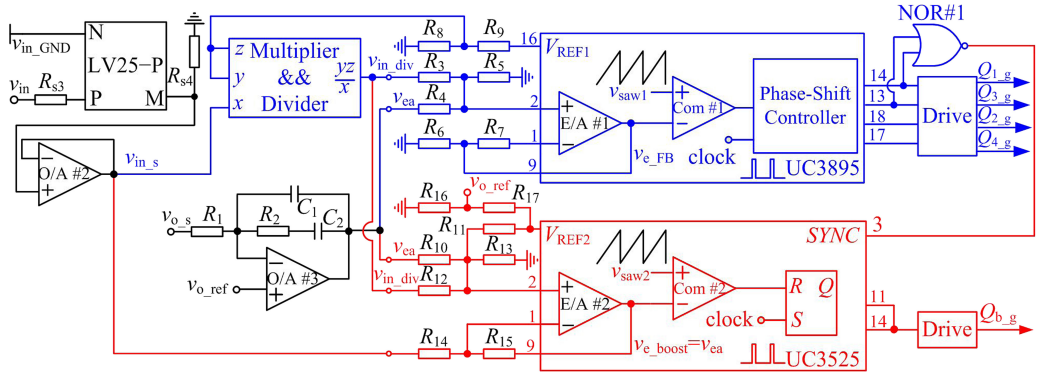

Fig. 17. Two-mode PS-TEM control with large-signal IVFF for FB-boost converter.

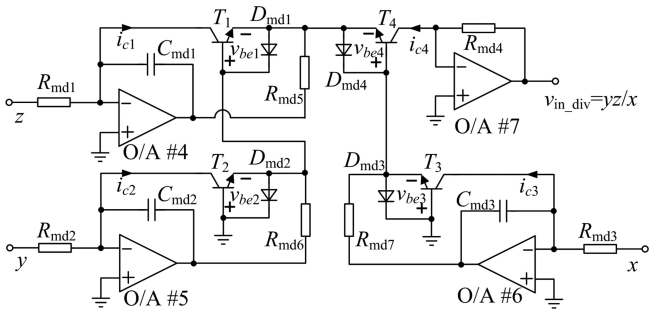

Fig. 18. Circuit of Multiplier&&Divider.

compensation. Fig. 18 is the specific circuit of the Multiplier&&Divider, where OA #4 $\sim$ #6 and triodes $T_1 \sim T_3$ is used to achieve logarithm operation, OA #7 and triode T_4 is used to achieve the inverse logarithm operation, and capacitors $C_{\mathrm{md1}} \sim C_{\mathrm{md3}}$ and resistors $R_{\mathrm{md1}} \sim R_{\mathrm{md4}}$ are used to improve the stability of this circuit. According to Fig. 17, the modulation signals for FB and boost cells can be derived as (39), shown at the bottom of the page. Combining (30) and (39), the values of $R_{10} \sim R_{15}$ in Fig. 17 can be obtained as $R_{10} = 1$ kΩ, $R_{11} = 2$ kΩ, $R_{12} = 43$ kΩ, $R_{13} = 5.6$ kΩ, $R_{14} = 10$ kΩ, $R_{15} = 6.8$ kΩ.

Fig. 19 shows the experimental waveforms of the FB-boost converter under the two-mode PS-TEM control scheme with IVFF compensation at steady state, including the primary voltage v_{AB}, rectified voltage v_{rec}, primary current i_{p} of the FB cell, and drain-to-source voltage of Q_{b} of the boost cell $v_{\mathrm{ds\_Qb}}$, from the top to bottom in each figure. Fig. 19(a) shows the waveforms at $V_{\mathrm{in}} = 500$ V, corresponding to FB-boost converter operating in FB mode, where Q_{b} is always off and $v_{\mathrm{ds\_Qb}}$ equals the output voltage, and the FB cell is controlled to regulate the

$$
\begin{cases}
v_{\mathrm{e\_FB}} = \left(\dfrac{R_7}{R_6}+1\right)\dfrac{R_5\left(R_4 v_{\mathrm{in\_div}} + R_3 v_{\mathrm{ea}}\right)}{R_4R_5+R_3R_4+R_3R_5} = \left(\dfrac{R_7}{R_6}+1\right)\dfrac{R_5}{R_4R_5+R_3R_4+R_3R_5}\left[R_4\left(\dfrac{R_8 V_{\mathrm{REF1}}}{R_8+R_9}\right)^2\dfrac{1}{v_{\mathrm{in\_s}}} + R_3 v_{\mathrm{ea}}\right] \\
v_{\mathrm{e\_boost}} = \left(\dfrac{R_{15}}{R_{14}}+1\right)\dfrac{R_{13}\left(R_{10}R_{12}V_{\mathrm{REF}} + R_{11}R_{12}v_{\mathrm{ea}} + R_{10}R_{11}v_{\mathrm{in\_div}}\right)}{R_{10}R_{11}R_{12}+R_{10}R_{12}R_{13}+R_{11}R_{12}R_{13}+R_{10}R_{11}R_{13}} - \dfrac{R_{15}}{R_{14}}v_{\mathrm{in\_s}} \\
\quad = \left(\dfrac{R_{15}}{R_{14}}+1\right)\dfrac{R_{13}\left[R_{10}R_{12}V_{\mathrm{REF}} + R_{11}R_{12}v_{\mathrm{ea}} + R_{10}R_{11}\left(\frac{R_8 V_{\mathrm{REF2}}}{R_8+R_9}\right)^2\frac{1}{v_{\mathrm{in\_s}}}\right]}{R_{10}R_{11}R_{12}+R_{10}R_{12}R_{13}+R_{11}R_{12}R_{13}+R_{10}R_{11}R_{13}} - \dfrac{R_{15}}{R_{14}}v_{\mathrm{in\_s}}
\end{cases}
\tag{39}
$$

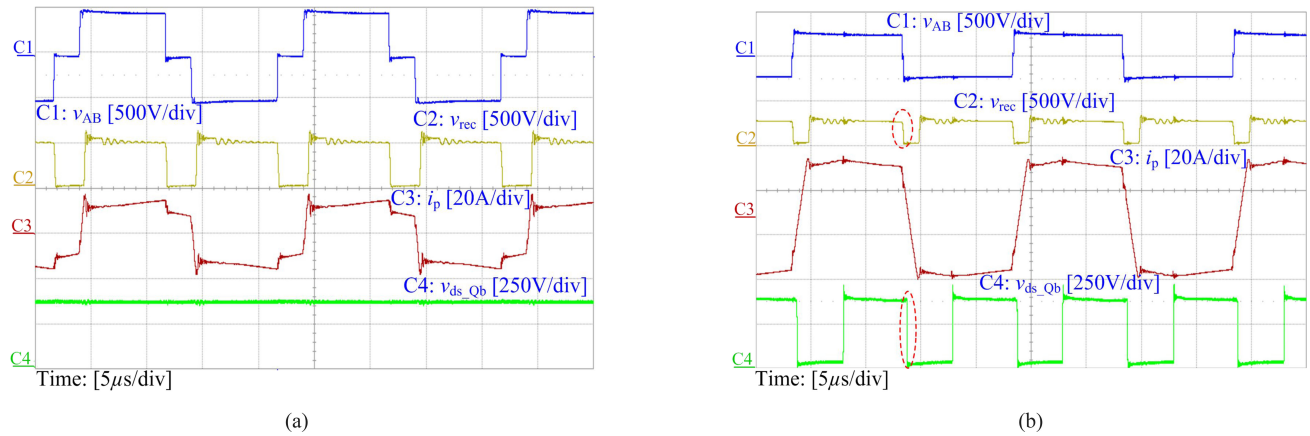

Fig. 19. Waveforms under the two-mode PS-TEM control scheme with IVFF at the steady state. (a) FB mode. (b) Boost mode.

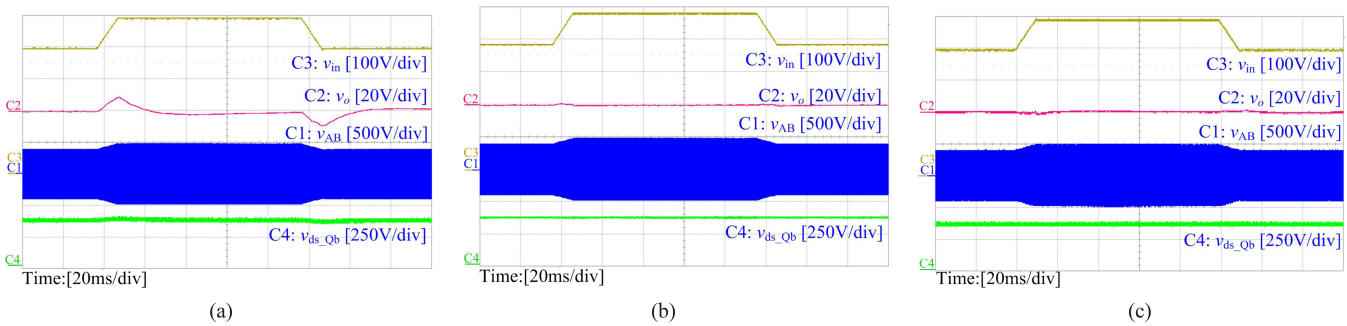

Fig. 20. Waveforms of step input voltage in FB mode. (a) Without IVFF. (b) With small-signal IVFF. (c) With large-signal IVFF.

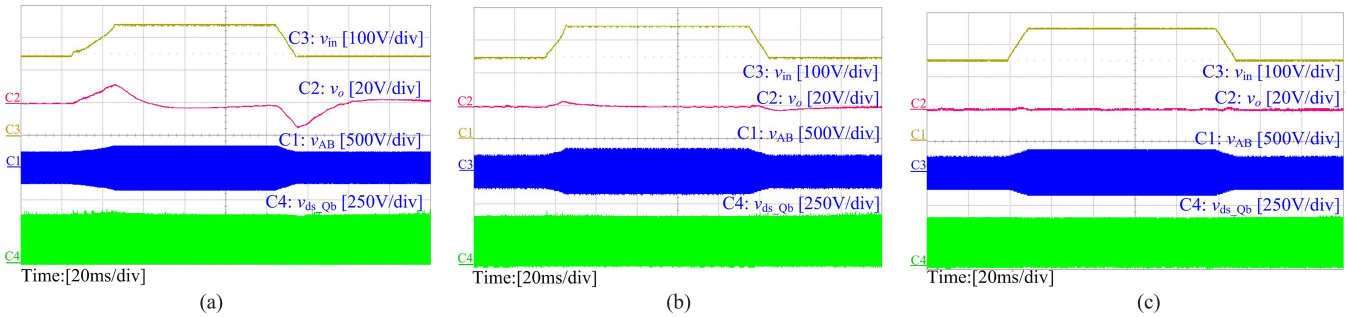

Fig. 21. Waveforms of step input voltage in boost mode. (a) Without IVFF. (b) With small-signal IVFF. (c) With large-signal IVFF.

output voltage. Fig. 19(b) shows the waveforms at $V_{\rm in} = 250$ V, corresponding to the converter operating in boost mode, where FB cell operates at full duty cycle and the output voltage is regulated by controlling $Q_{\rm b}$. Also, it can be seen from the dashed cycles of the waveforms $v_{\rm rec}$ and $v_{\rm ds\_Qb}$ shown in Fig. 19(b) that $Q_{\rm b}$ is always on when the leading switches Q_1 and Q_3 are off, which means that the PS-TEM strategy mentioned in Section II is achieved for the FB-boost converter, as explained in [10].

Figs. 20–22 show the experimental waveforms at full load with and without IVFF compensations when the input voltage steps between 400 and 500 V, 250 and 350 V, and 250 and 500 V, respectively, corresponding to the FB-boost converter operating in FB mode, boost mode, and the shifting between FB and boost modes. In addition, (a), (b), and (c) in these figures are corresponding to the two-mode PS-TEM control scheme without, with small-signal, and with large-signal IVFF compensations, respectively. As seen, both the two-mode PS-TEM control schemes with small-signal and large-signal IVFF compensations can achieve automatic selections of correct operating mode and the corresponding IVFF compensation simultaneously, and then the input voltage transient response over the entire input voltage range is improved. Moreover, as seen, the two-mode PS-TEM control scheme with large-signal IVFF compensation can achieve smoother shifting between FB mode and boost mode. It should be explained that the stepped input voltage is from the programmable dc source, Chroma 62150H-600S, with maximum output current 25 A and output voltage 600 V. Once the required current of the converter is greater than 25 A, the slew rate of the step input voltage will be limited. As shown in Figs. 21–22, the slew rate of the input

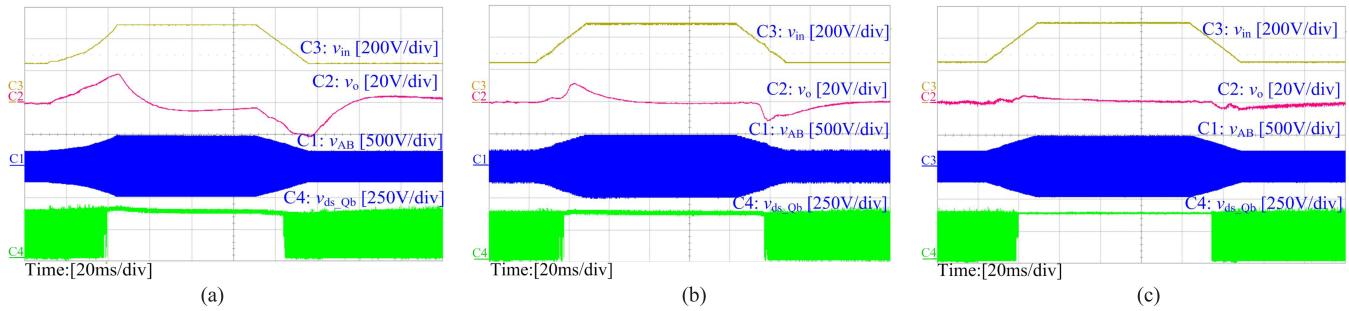

Fig. 22. Waveforms of step input voltage between FB and boost modes. (a) Without IVFF. (b) With small-signal IVFF. (c) With large-signal IVFF.

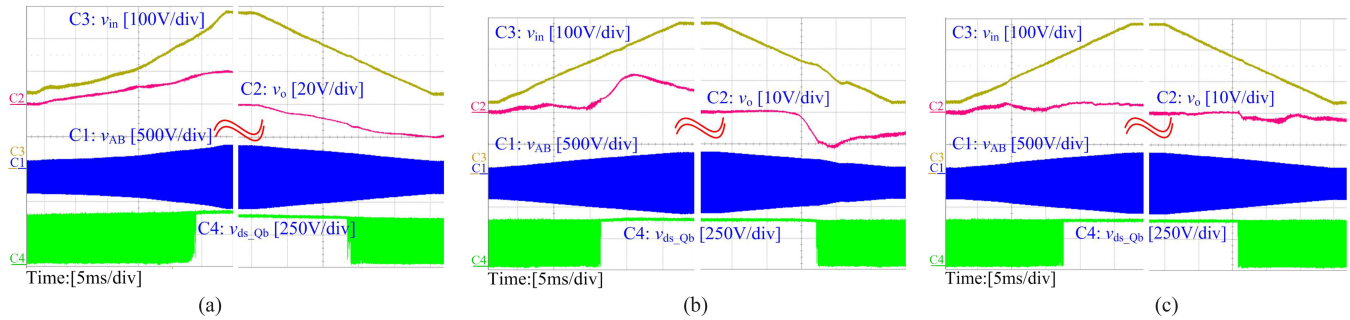

Fig. 23. Zoom of step input voltage between FB and boost modes. (a) Without IVFF. (b) With small-signal IVFF. (c) With large-signal IVFF.

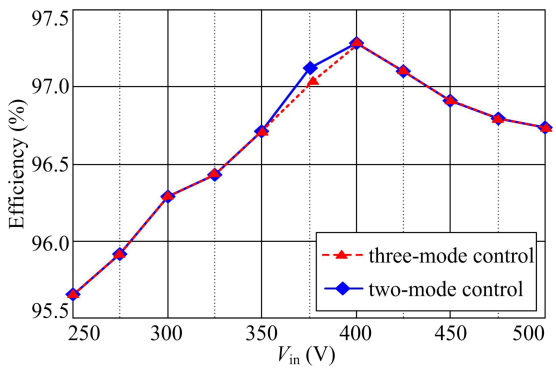

Fig. 24. Efficiency of FB-boost converter in the full load condition.

voltage without IVFF compensation is smaller than that with IVFF compensation, when the stepped input voltage between 250 and 350 V, or 250 and 500 V happens. This reason is that the input current of the converter without IVFF compensation is greater than 25 A in these conditions. In order to observe the transition between FB and boost modes more clearly, Fig. 23 gives a zoom of Fig. 22. Specifically, (a), (b), and (c) are corresponding to the two-mode PS-TEM control scheme without, with small-signal, and with large-signal IVFF compensations, respectively.

The efficiency of the FB-boost converter under the two-mode PS-TEM control scheme with IVFF compensation in the full load condition is measured, as the solid line shown in Fig. 24, which is the same as the condition without IVFF compensation. In addition, the dashed line in Fig. 24 shows the efficiency of the FB-boost converter with the control scheme in [10]. As seen, the FB-boost converter under the proposed control schemes achieves high efficiency over the entire input voltage range, especially at the mode-shifting point, and the efficiency in this paper is higher than it in [10] due to the FB-boost mode.

VIII. Conclusion

A two-mode PS-TEM control scheme with automatic mode-shifting ability is adopted to achieve high efficiency and automatic shifting between FB and boost modes for the FB-boost converter. Furthermore, the small-signal model of this converter is built and the IVFF functions under different operating modes are derived. Considering the small-signal and large-signal control laws of the derived IVFF functions, the two-mode PS-TEM control schemes with small-signal and large-signal IVFF compensations are then proposed, respectively, both of which can achieve automatic selection of operating modes and the corresponding IVFF compensations, simultaneously. Especially, for the control scheme with large-signal IVFF compensation, more accurate IVFF compensation and smoother mode shifting are guaranteed. Moreover, reasonable simplification of the large-signal IVFF compensation in boost mode is discussed for easy implementation. Besides, the comparisons between the two-mode PS-TEM control schemes with small-signal, large-signal, and without IVFF compensations, including the output signals of the voltage regulator, the input-to-output voltage transfer functions, and implementations, are presented for clear description. Finally, a 250–500-V input, 360-V output, and 6-kW-rated power prototype is built and tested, and the experimental results demonstrate the validity of the proposed control schemes, with which both high efficiency and improved input transient response over the whole input voltage range are achieved.

REFERENCES

[1] F. Luo and D. Ma, "Design of digital tri-mode adaptive-output buck-boost power converter for power-efficient integrated systems," *IEEE Trans. Ind. Electron.*, vol. 57, no. 6, pp. 2151–2160, Jun. 2010.

[2] R. W. Erickson and D. Maksimovic, *Fundamentals of Power Electronics*. Norwell, MA USA: Kluwer, 2011.

[3] X. Ren, X. Ruan, H. Qian, M. Li, and Q. Chen, "Three-mode dual-frequency two-edge modulation scheme for four-switch buck-boost converter," *IEEE Trans, Power Electron.*, vol. 24, no. 2, pp. 499–509, Feb. 2009.

[4] C. Wei, C. Chen, K. Wu, and I. Ko, "Design of an average-current-mode noninverting buck-boost dc-dc converter with reduced switching and conduction losses," *IEEE Trans. Power Electron.*, vol. 27, no. 12, pp. 4934–4943, Dec. 2012.

[5] D. C. Jones and R. W. Erickson, "A nonlinear state machine for dead zone avoidance and mitigation in a synchronous noninverting buck-boost converter," *IEEE Trans. Power Electron.*, vol. 28, no. 1, pp. 467–480, Jan. 2013.

[6] G. K. Andersen and F. Blaabjerg, "Current programmed control of a single-phase two-switch buck-boost power factor correction circuit," *IEEE Trans. Power Electron.*, vol. 53, no. 1, pp. 263–271, Feb. 2006.

[7] H. Liao, T. Liang, L. Yang, and J. Chen, "Non-inverting buck-boost converter with interleaved technique for fuel-cell system," *IET Power Electron.*, vol. 5, no. 8, pp. 1379–1388, Sep. 2012.

[8] H. Xiao and S. Xie, "Interleaving double-switch buck-boost converter," *IET Power Electron.*, vol. 5, no. 6, pp. 899–908, Jul. 2012.

[9] Y. J. Lee, A. Khaligh, A. Chakraborty, and A. Emadi, "Digital combination of buck and boost converters to control a positive buck-boost converter and improve the output transients," *IEEE Trans. Power Electron.*, vol. 24, no. 5, pp. 1267–1279, May 2009.

[10] C. Yao, X. Ruan, and X. Wang, "Isolated buck-boost dc/dc converters suitable for wide input-voltage range," *IEEE Trans. Power Electron.*, vol. 26, no. 9, pp. 2599–2613, Sep. 2011.

[11] T. Ishii, M. Yoshida, M. Motomori, and J. I. Hara, "Buck-boost converter," U.S. Patent 7268525, 2007.

[12] Y. J. Lee, A. Khaligh, A. Chakraborty, and A. Emadi, "A compensation technique for smooth transitions in a noninverting buck-boost converter," *IEEE Trans. Power Electron.*, vol. 24, no. 4, pp. 1002–1016, Apr. 2009.

[13] C. Restrepo, T. Konjedic, J. Calvente, M. Milanovic, and R. Giral, "Fast transitions between current control loops of the coupled-inductor buck-boost dc-dc switching converter," *IEEE Trans. Power Electron.*, vol. 28, no. 8, pp. 3648–3652, Aug. 2013.

[14] C. Restrepo, J. Calvente, A. Cid-Pastor, A. E. Aroudi, and R. Giral, "A noninverting buck-boost dc-dc switching converter with high efficiency and wide bandwidth," *IEEE Trans. Power Electron.*, vol. 26, no. 9, pp. 2490–2503, Sep. 2011.

[15] B. Arbetter and D. Maksimovic, "Feedforward pulse width modulators for switching power converters," *IEEE Trans. Power Electron.*, vol. 12, no. 2, pp. 361–368, Mar. 1997.

[16] M. Chen and J. Sun, "Feedforward current control of boost single-phase PFC converters," *IEEE Trans. Power Electron.*, vol. 21, no. 2, pp. 338–345, Mar. 2006.

[17] D. M. Van de Sype, K. De Gusseme, A. P. M. Van den Bossche, and J. A. Melkebeek, "Duty-ratio feedforward for digitally controlled boost PFC converters," *IEEE Trans. Ind. Electron.*, vol. 52, no. 1, pp. 108–115, Feb. 2005.

[18] P. C. Huang, W. Q. Wu, H. H. Ho, and K. H. Chen, "Hybrid buck-boost feedforward and reduced average inductor current techniques in fast line transient and high-efficiency buck-boost converter," *IEEE Trans. Power Electron.*, vol. 25, no. 3, pp. 719–730, Mar. 2010.

[19] J. J. Chen, P. N. Shen, and Y. S. Hwang, "A high efficiency positive buck-boost converter with mode-select circuit and feed-forward techniques," *IEEE Trans. Power Electron.*, vol. 28, no. 9, pp. 4240–4247, Sep. 2013.

[20] F. Guo, L. Fu, C. Lin, C. Li, W. Choi, and J. Wang, "Development of an 85-kW bidirectional quasi-Z-Source inverter with dc-link feed-forward compensation for electric vehicle applications," *IEEE Trans. Power Electron.*, vol. 28, no. 12, pp. 5477–5488, Dec. 2013.

[21] C. Yao, X. Ruan, W. Cao, and P. Chen, "A two-mode control scheme with input voltage feed-forward for two-switch buck-boost dc-dc converter," *IEEE Trans. Power Electron.*, vol. 29, no. 4, pp. 2037–2048, Apr. 2014.

[22] D. V. Otto, "Reduction of switching regulator audiosusceptibility to zero," *IEE Electron. Lett.*, vol. 22, no. 8, pp. 441–442, Apr. 10, 1986.

[23] M. Karppanen, T. Suntio, and M. Sippola, "Dynamical characterization of input-voltage-feedforward-controlled buck converter," *IEEE Trans. Ind. Electron.*, vol. 54, no. 2, pp. 1005–1013, Apr. 2007.

[24] R. Redl and N. O. Sokal, "Optimizing dynamic behavior with input and output feed-forward and current-mode control," in *Proc. Powercon7*, San Diego, CA, USA, 1980, pp. H1-1–H1-16.

[25] R. Redl and N. O. Sokal, "Near-optimum dynamic regulation of dc-dc converters using feed-forward of output current and input voltage with current-mode control," *IEEE Trans. Power Electron.*, vol. PE-1, no. 3, pp. 181–192, Jul. 1986.

[26] V. Vlatkovic, J. A. Sabate, R. B. Ridley, F. C. Lee, and B. H. Cho, "Small-signal analysis of the phased-shifted PWM converter," *IEEE Trans. Power Electron.*, vol. 7, no. 1, pp. 128–135, Jan. 1992.

[27] Y. Liu and P. C. Sen, "A general unified large signal model for current programmed dc-to-dc converters," *IEEE Trans. Power Electron.*, vol. 9, no. 4, pp. 414–424, Jul. 1994.

[28] M. K. Kazimierczuk and D. Czarkowski, "Energy-conservation approach to modeling PWM dc-dc converters," *IEEE Trans. Aerosp. Electron. Syst.*, vol. AES-29, no. 3, pp. 1059–1063, Jul. 1993.

Chuan Yao received the B.S. degree in the electrical engineering and automatization from Chongqing University, Chongqing, China, in 2007, and the Ph.D. degree from the College of Electrical and Electronic Engineering, Huazhong University of Science and Technology, Wuhan, China, in 2013.

He is currently an Engineer in the Wuhan Second Ship Design and Research Institute, Wuhan. His main research interests include soft-switching dc–dc converters and renewable energy generation system.

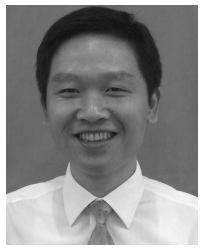

Xinbo Ruan (M'97–SM'02) received the B.S. and Ph.D. degrees in electrical engineering from Nanjing University of Aeronautics and Astronautics (NUAA), Nanjing, China, in 1991 and 1996, respectively.

In 1996, he joined the Faculty of Electrical Engineering Teaching and Research Division, NUAA, where he became a Professor in the College of Automation Engineering in 2002 and has been engaged in teaching and research in the field of power electronics. From August to October 2007, he was a Research Fellow in the Department of Electronic and Information Engineering, Hong Kong Polytechnic University, Hong Kong, China. Since March 2008, he has been also with the School of Electrical and Electronic Engineering, Huazhong University of Science and Technology, China. He is a Guest Professor with Beijing Jiaotong University, Beijing, China, Hefei University of Technology, Hefei, China, and Wuhan University, Wuhan, China. He is the author or coauthor of five books and more than 180 technical papers published in journals and conferences. His main research interests include soft-switching dc–dc converters, soft-switching inverters, power factor correction converters, modeling the converters, power electronics system integration, and renewable energy generation system.

Dr. Ruan received the Delta Scholarship by the Delta Environment and Education Fund in 2003 and received the Special Appointed Professor of the Chang Jiang Scholars Program by the Ministry of Education, China, in 2007. From 2005 to 2013, he had served as a Vice President of the China Power Supply Society, and since 2008, he has been a member of the Technical Committee on Renewable Energy Systems within the IEEE Industrial Electronics Society. He has been an Associate Editor for the IEEE TRANSACTIONS ON INDUSTRIAL ELECTRONICS and the IEEE JOURNAL OF EMERGING AND SELECTED TOPICS ON POWER ELECTRONICS since 2011 and 2013, respectively. He is a Senior Member of the IEEE Power Electronics Society and the IEEE Industrial Electronics Society.

Xuehua Wang (M'12) received the B.S. degree in electrical engineering from Nanjing University of Technology, Nanjing, China, in 2001, and the M.S. and Ph.D. degrees in electrical engineering from Nanjing University of Aeronautics and Astronautics (NUAA), Nanjing, in 2004 and 2008, respectively.

He is currently a Lecturer in the School of Electrical and Electronic Engineering, Huazhong University of Science and Technology, Wuhan, China. His main research interests include multilevel inverter and renewable energy generation system.